UNIVERSITY OF CALIFORNIA, MERCED

Deuterium Kinetic Isotope Effects as Mechanistic Probes for Synthetically Useful Cyclic Hydrogen Transfers

A dissertation submitted in partial satisfaction of the
requirements for the degree Doctor of Philosophy

in

Chemistry and Chemical Biology

by

Xiao Li

Committee in Charge:

Professor Benjamin J. Stokes, Chair

Professor Andy LiWang

Professor Matthew P. Meyer, Advisor

Professor Jason Hein

The Dissertation of Xiao Li is approved, and it is acceptable in quality and form for publication on microfilm and electronically:

Professor Andy LiWang

Professor Matthew P. Meyer

Professor Jason Hein

Professor Benjamin J. Stokes (Chair)

University of California, Merced

2016

DEDICATION

I dedicate this dissertation to the ambition and resilience I have developed in the past of my life, without which I could not have completed this work. I could not gain the strength of my mind and body without my parents, my husband Ding Li, my other family members, friends and mentors who supported me along the way. I would like to express my deepest gratitude to my parents who always encourage me to live up to my full potential. I deeply thank my husband Ding Li whose love and generosity to me is one of the most important sources of my passion to the world.

TABLE OF CONTENTS

LIST OF ABBREVIATION

KIE	kinetic isotope effect
TS	transition state
TST	transition state theory
ZPE	zero-point energy
RGM	the rule of the geometric mean
CVT	canonical variational transition state theory
SCT	small curvature tunneling
NMR	nuclear magnetic resonance
SMD	solvation model based on density
LFER	linear free energy relationship
THF	tetrahydrofuran
DMSO	dimethyl sulfoxide
RBF	round bottom flask
TLC	think layer chromatography
FID	free induction decay
S/N	signal to noise ratio

LIST OF FIGURES

LIST OF TABLES

ACKNOWLEDGEMENTS

I acknowledge my advisor Prof. Matthew P. Meyer for providing me an opportunity to study and perform research on physical organic chemistry. His patience and guidance have nurtured me to become an independent and confident chemist from a freshly graduated college student from China. The skills I gained in his lab are valuable and transferrable for the future career I pursue.

I acknowledge my committee member Prof. Andy LiWang for providing advice and technical support in using the Bruker 600 MHz NMR for research in chapter two and four. He and his group are always friendly and supportive, which makes the journal of my Ph.D. training much more enjoyable.

I acknowledge the external member and also the former chair of my committee prof. Jason Hein for providing me useful advice on organic synthesis and graduate school research career plan in the first three years of my graduate study at UC Merced.

I acknowledge the chair of my committee prof. Benjamin J. Stokes for providing constructive feedback in my committee meetings and for mentoring me in teaching Chem 8L lectures in the summer of 2016.

I acknowledge the CCB faculty members Prof. Michael Colvin, Prof. Hrant Hratchian and Prof. Anne Kelly for providing graduate level courses to prepare me with knowledge and skills needed by my graduate and future research.

I acknowledge Prof. Erik Menke for informing me the opportunity the dissertation fellowship application.

I gratefully thank my previous coworkers: Dr. Thomas Giagou, Dr. Shuhuai Xiang and Dusty Ventura for sharing their knowledge, wisdom and time in the laboratory with me.

I would like to thank Dr. Makenzie R. Provorse for providing useful advice on using the POLYRATE program for the research in chapter one.

I gratefully thank CCB department for the summer fellowship in 2012-2015, and for the travel award in 2014.

I gratefully thank the Graduate Division for the Dean’s dissertation fellowship in 2016.

CURRICULUM VITA

Education

Aug 2011-current	Ph.D. candidate in Physical Organic Chemistry University of California, Merced
2007-2011	B.S. in Applied Biology City University of Hong Kong (Hong Kong SAR)
Jan to June 2010	visiting student University of Dundee (United Kingdom)

Publication

"Quantum Suppression of Intramolecular Deuterium Kinetic Isotope Effects in a Pericyclic Hydrogen Transfer Reaction" Xiao Li and Matthew P. Meyer, *J. Am. Chem. Soc*. (submitted)

ABSTRACT

Hydrogen transfer reactions are among the most fundamental organic reactions. They are involved in nearly all enzyme-catalyzed reactions necessary for the sustenance of life, and they are often involved in key steps in synthetically useful reductions. Notable among synthetically useful reactions are the class of reactions known as C–H bond functionalization. It is surprising, then, that this most fundamental chemical event is so poorly understood. To address this knowledge gap, we have developed new experimental and computational approaches that allow interrogation of the core physical nature of cyclic hydrogen transfer reactions. In general, our laboratory utilizes kinetic isotope effects (KIEs) to probe chemical reactions. This technique involves accurately determining how replacement of atoms with their heavier isotopes affects the reaction rate (or product distribution). In order to extract the most insightful information from KIE studies, suitable experiments and measurement methods need to be well-designed and carefully executed.

This dissertation is composed of four chapters. The first chapter serves as a general introduction that lays out the background of the mechanistic study of cyclic hydrogen transfer, the concepts of kinetic isotope effect and a concise review of traditional and new techniques that utilize KIEs to elucidate reaction mechanisms. The remaining chapters present three unique studies that culminate in a unified view of cyclic hydrogen transfers. Each study is designed to interrogate the key physical aspects of a synthetically useful and mechanistically interesting hydrogen transfer. The first study explores the Chugaev elimination, which is used to transform alcohols into alkenes in a typically regioselective manner. In this study, we have used a combination of intermolecular and intramolecular ^{2}H KIE measurements to demonstrate that this reaction is dominated by quantum mechanical behavior even though it occurs at elevated temperatures. Comparison between the experimental and computational results imply that the observed KIEs are influenced by the location of the bottleneck (or transition state) which is found to be dependent on the isotopic substitution. Chapter 3 explores the Cope elimination, which can be used to install alkenes adjacent to an amine, demonstrated that seemingly simple cyclic hydrogen transfer reactions can proceed simultaneously via multiple mechanisms depending upon driving force and temperatures. Our approaches in the Cope and Chugaev eliminations were then utilized to explore an exciting new C–H functionalization reaction developed by DuBois. This study demonstrates that cyclic H-transfers mediated by a Ru-nitrene species are fundamentally similar to relatively simpler syn-β eliminations in terms of the involvement of quantum mechanical phenomena. The reaction models built with prototype reactions can be generalized to more complicated metal catalyzed reactions to facilitate a better understanding of the reaction in terms of both reactivity and selectivity.

Chapter 1. Introduction and Background

1.1. Importance of Reaction Mechanisms

An accurate understanding of the reaction mechanism has the potential to enable rational reaction design. A reaction mechanism describes the fundamental changes in bonding that accompany the conversion of reactant(s) into product(s) during a chemical reaction.[1] In the context of a reaction pathway, perfect understanding of reaction mechanism informs the depiction of the geometry and energies of the reacting molecule(s) at each stage of the reaction process.[1]

Reaction mechanism plays an important role in guiding drug design, synthetic methodology, and theoretical model refinement. Firstly, knowing the transition structure (TS) of an enzymatic reaction allows scientists to design transition state mimics as inhibitors, which have the potential to become biologically active drugs. For example, Schramm et al. designed several enzyme inhibitors according to the transition state structure constructed from kinetic isotope effect studies.[2-4] Secondly, in small organic molecule chemistry, the reaction mechanism does not only provide an arrow pushing scheme of a reaction but also provides insight into the factors that govern the reactivity and selectivity of a reaction, the latter of which is indispensable for designing the catalyst, reagents and conditions for a given synthetic process.[1,5,6] Last but not least, the mechanistic study tests the limit of theoretical models and thus helps to advance the field of theoretical chemistry. The rate and product distribution of organic reactions are now mainly explained and predicted by the transition state theory (TST) developed by Eyring.[7] However, it has been found that TST fails to predict the experimental results when a dynamical effect or quantum mechanical effect is significant (when the deviation of reaction rate or selectivity from TST is so great and cannot be accounted for by experimental error).[8,9] As a result, exploring the mechanism of reactions that do not obey TST should offer more data upon which more refined computational methods can be conceived.

As discussed above, reaction mechanism is essential to understaning both enzymatic reactions and small molecule organic reactions. This dissertation focuses on studying the mechanism of small molecule organic reactions. In particular, the basic origins of the kinetic isotope effect as a mechanistic tool will be developed and then applied in the context of three fundamental hydrogen transfer reactions.

1.2. Hydrogen Transfer Reactions: Importance, Limitations in Current Understanding and the Scope of this Dissertation

Hydrogen transfer is perhaps the most fundamental and ubiquitous process in biochemical and synthetically useful reactions. In biological systems, hydrogen transfer is important in the transferring of a reducing equivalent from the cofactors to the substrates in oxidoreductase-catalyzed reactions, which is one of the major categories of enzymatic

reactions. Hydrogen transfer also characterizes proton transfers, which accompany the manifold general acid-catalyzed reaction steps found in enzyme mechanism. In synthetic chemistry, hydrogen transfer is inherent to transformations ranging from β-hydride eliminations to organocatalytic reactions, to C-H functionalizations accomplished using metal carbenoid or nitrenoid species.

Quantum mechanical behavior frequently has significant effects on hydrogen transfer processes due to the substantial wave-like properties of the hydrogen atom, as predicted by the de Broglie wavelength ($\lambda=h/(2mE)^{1/2}$. Relatively thorough experimental studies and reliable theoretical models were carried out and built for proton-coupled electron transfer (PCET)[10,11] and atom-diatomic collinear reactions[12]. Surprisingly, the quantum tunneling effects remain poorly understood for many heterolytic polyatomic reactions. As a result, many current models for enzyme-catalyzed and synthetic reactions are lacking in physical detail.

In order to address the knowledge gap, our laboratory has put effort into studying the tunneling phenomena in cyclic hydrogen transfer reactions, which involve a cyclic transition structure (usually a five-membered or six-membered ring) that contains the hydrogen donor, the transferred hydrogen atom and the hydrogen acceptor in one fragment. The cyclic transition structure is a common feature in intramolecular eliminations and catalyst-substrate complex reactions. Enzymatic hydrogen transfer does not necessarily go through a cyclic transition state, but it is effectively an intramolecular process that occurs within the enzyme-substrate 'supermolecule'.[13] Because of the similarities between enzyme-catalyzed reactions and unimolecular reactions, insights gained from our research can find applicability to systems as diverse as new synthetic methodologies to the development of more refined transition state mimic inhibitors.

In this dissertation, the author will present three mechanistic studies: two on intramolecular eliminations (Figure 1 A, B) and one on ruthenium catalyzed C-H amination (Figure 1 C).

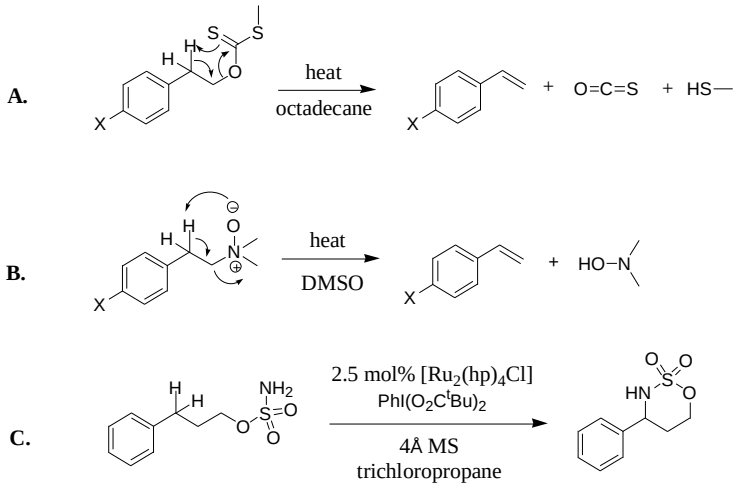

Figure 1. Reactions studied in this dissertation. A) Chugaev elimination; B) Cope elimination; C) C-H amination catalyzed by ruthenium catalyst.

1.3.General Introduction to Kinetic Isotope Effect

Kinetic isotope effect (KIE) is an effect in which the isotope substitution changes the reaction rate.[1] By convention, KIE is reported as a ratio of rate constants between light and heavy isotopologues (compounds of identical chemical composition but which differ only in isotopic composition) or isotopomers (isomers having the same number of each isotopic atom but differing in their positions (Equation 1).[14]

$$KIE = k_{light}/k_{heavy} \qquad \textit{Equation 1}$$

KIEs have been observed for numerous isotopic pairs of elements, including hydrogen ($^{1}H/^{2}H$; $^{1}H/^{3}H$), carbon ($^{12}C/^{13}C$; $^{12}C/^{14}C$), oxygen ($^{16}O/^{18}O$; $^{16}O/^{17}O$), nitrogen ($^{14}N/^{15}N$) and chlorine ($^{35}Cl/^{37}Cl$)[14], among which ^{2}H KIE (k_H/k_D) is relatively large in magnitude and easier to measure compared to that of other heavy atoms. ^{2}H KIE is also the most suitable mechanistic tool for studying hydrogen transfer reactions. This dissertation will solely focus on the discussion of ^{2}H KIE. KIEs are classified into primary and secondary KIE, and the definition and application of each type will be elaborated in the following subsections.

1.3.1. Primary Kinetic Isotope Effect

Primary kinetic isotope effects (often written as 1° KIE) are attributed to bond breaking or forming at the isotopic substitution site.[14] The origin of 1° KIEs can be illustrated by the simplified model shown in Figure 2A. Kinetic isotope effect arises from the zero-point energy (ZPE) difference in chemical bonds between protiated and deuterated reactants, and is indeed a quantum mechanical phenomenon. According to the Born-Oppenheimer

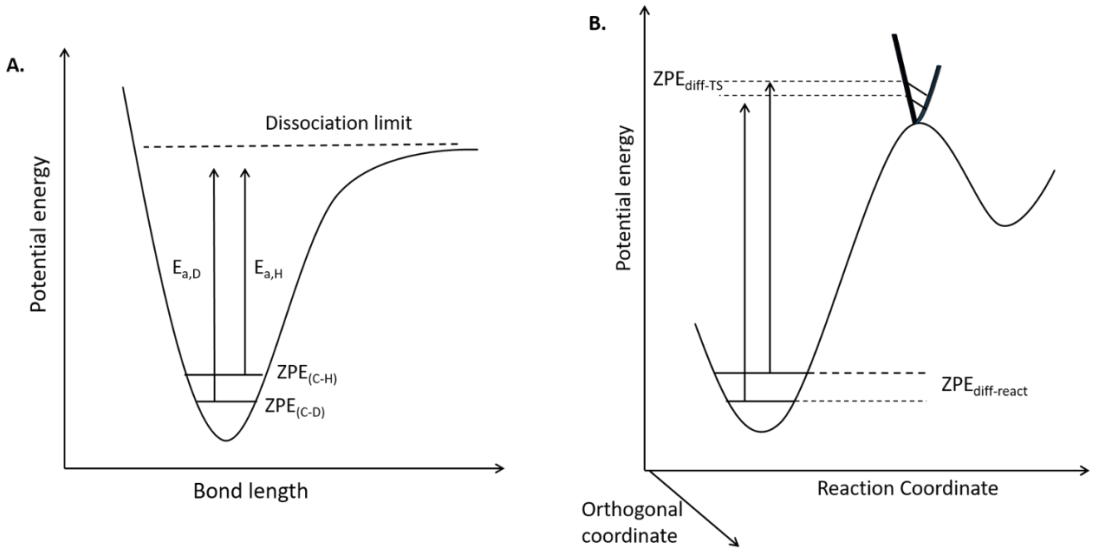

Figure 2. Diagrams illustrating the origin primary KIE. A) The potential energy diagram of a carbon-hydrogen bond with zero-point energy levels for H and D shown. B) A reaction coordinate diagram showing that a residual ZPE difference between C-H and C-D bonds at the TS diminishes the isotope effect.[1]

principle, the potential energy surface of a reaction does not change with isotopic substitution.[15] In a quantum mechanical world, the energy stored in chemical bonds is quantized and the ground state energy (zero-point energy) of a harmonic oscillator is proportional to the vibrational frequency (*Equation 2*).

$$ZPE = \frac{1}{2} hc\nu \qquad \textit{Equation 2}$$

$$\nu = \frac{1}{2\pi c} \cdot \sqrt{\frac{k_f}{\mu}} \qquad \textit{Equation 3}$$

$$k = A(T) \cdot e^{-E_a/RT} \qquad \textit{Equation 4}$$

$$KIE = \frac{k_H}{k_D} = \frac{A_H}{A_D} \cdot e^{(E_{a,D} - E_{a,H})/RT} \qquad \textit{Equation 5}$$

Here h is Planck's constant, c is the speed of light and $\tilde{\nu}$ is the frequency of a bond vibration in wavenumber (cm^{-1}). *Equation 3* indicates that the frequency is proportional to the square root of the force constant k_f, and is inversely proportional to the square root of the reduced mass (for a diatomic molecule: $\mu = m_1 \cdot m_2/(m_1+m_2)$) . The force constant is the same for a C-H bond and a C-D bond, while the reduced mass is greatly affected by the mass of the hydrogen atom (similar to other heavy atom-hydrogen bond, e.g. O-H, N-H, etc.). Substituting proton with deuterium increases the reduced mass, and thus lowers the zero-point energy as shown in Figure 2A.[1] Assuming the bond of interest is completely broken and has no vibration at the transition state, the activation energy (E_a) is determined by the reactant zero-point energy: deuterated compound has smaller zero-point energy and hence larger activation energy ($E_{a,D}$-$E_{a,H}$=$ZPE_{C\text{-}H}$-$ZPE_{C\text{-}D}$). According to the Arrhenius equation (*Equation 4*), the reaction with greater energy barrier (activation energy) reacts slower. The assumptions in *Equation 4* are simplistic, however. A more comprehensive model by Westheimer[16] demonstrates that the net effects of isotopic substitution are exerted on vibrations other than the stretching vibration of the bond that is cleaved (Figure 2B). When the assumption of complete loss of ZPE at the transition state is dropped, the KIE can be estimated using *Equation 5* from the activation energy difference, given that $A_H/A_D \approx 1$ without considering quantum tunneling. When the ZPE difference is smaller at the transition state than at the reactant state ($E_{a,D}$-$E_{a,H}$ = $ZPE_{diff\text{-}react}$-$ZPE_{diff\text{-}TS}$ >0), as it is in primary KIEs, the observed k_H/k_D is greater than one. A KIE that is greater than one is called normal KIE.

The semiclassical upper limit of primary KIE can be estimated by considering breaking a sp^3 carbon-hydrogen bond at 298K. The frequency of a sp^3 C-H bond stretching is around 3000 cm^{-1} and that of a C-D bond is 2200 cm^{-1}.[17] Substituting the frequencies into *Equation 2* and *Equation 5* gives a KIE of 6.9 at 298K (p. 26 in Ref.[15]). If the bending modes are also

considered and assumed to be totally lost at TS, the upper limit of *1° KIE* is predicted to be 15~20 (p. 130 in Ref.[15]). Most observed KIEs are smaller than this maximum possible value because the bond that is cleaved in the reaction does not completely break at the transition state for most cases. In accordance with Westheimer's model (p. 426~428 in Ref.[1], [16]), reactions with unsymmetrical location of TS (strong endo- or exoenergetic reactions) or with bent TS have attenuated KIEs.

The primary KIE is a very powerful tool for mechanistic study, providing physical information that is peculiar to the bond forming/breaking process that cannot be obtained from other kinetic studies. A substantial primary KIE (usually 1° KIE > 2) is often accepted as an evidence of bond forming or breaking in the rate-determining step. The size of the KIE can also offer some clue to the nature of the bond breaking/forming event: hydrogen atom abstraction reactions are known to have relatively large 1° KIE (12~14, the larger than semiclassical limit value is attributed to tunneling), while hydride shift reactions have smaller 1° KIEs (≈2).[18] However, due to kinetic complexity, interpreting KIEs, especially in enzyme-catalyzed reactions, can be more complicated than just categorizing a KIE as being large, medium or small. A single KIE measurement is really a scalar measurement, providing only magnitude. Primary KIEs are sometimes measured as a function of temperature to generate an Arrhenius plot (ln(KIE) vs. 1/T). Arrhenius plots can yield further insight into the physical origins of observed KIEs[19], as will be discussed in the following subsections.

1.3.2. Secondary Kinetic Isotope Effect

Secondary kinetic isotope effects (2° KIE) arise from isotopic substitution at positions where no bond breaking or forming occurs. Similar to 1° KIEs, 2° KIEs result from the ZPE difference between C-H and C-D at TS versus the reactant ($E_{a,D}$-$E_{a,H}$ = $ZPE_{diff\text{-}react}$-$ZPE_{diff\text{-}TS}$). Since the isotopically labelled bond is not broken or made during the reaction, 2° KIE is produced from the vibrational modes that are orthogonal to the reaction coordinate and undergo change(s) during the transition from the reactant to the saddle point (Figure 2). Such changes usually include one or more of the following processes: (1) re-hybridization (e.g. $sp^3 \rightarrow sp^2$, $sp^2 \rightarrow sp^3$), (2) changes in hyperconjugation, and (3) the development or relief of steric repulsion.[14]

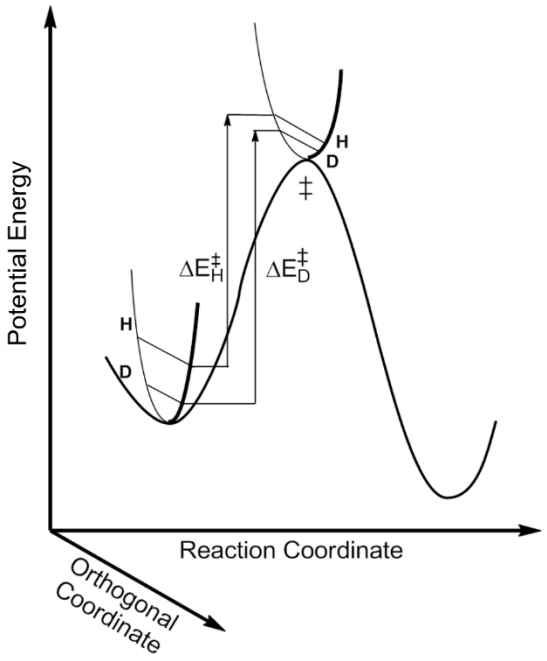

Figure 3. Potential energy diagram illustrating that the 2° KIE originates from the difference in ZPE contained in TS and the reactants.

Secondary KIEs can be either normal (KIE>1) or inverse (KIE<1). When the bonds proceed from a "tight" to a "loose" vibrational configuration, for example from sp^3 to sp^2 hybridization, a normal 2° KIE will be generated. Transition from "loose" to "tight" vibrations will yield an inverse 2° KIE. For example, when the bonds encounter steric repulsion at the transition state, the potential energy well is steeper and ZPE difference between C-H and C-D is larger at the transition state than at the reactant well. As a result, deuterated isotopologues react faster than protiated isotopologues when steric occlusion increases at the transition state relative to that present at the reactant state.

Despite its comparatively small magnitude, the 2° KIE has been found to be an information-rich observable with regards to the nature of the transition state.[20] As discussed above, 2° KIE can reflect the bond force constant changes arising from various physicochemical processes, and such information is very useful in developing cogent models of transition structure when interpreted in the context of chemical intuition.[20]

1.4.Quantum Mechanical Effects Upon Hydrogen Transfer

1.4.1. The Nature and Physical Principles of Quantum Tunneling

Section 1.3 discussed the influences of one type of quantum mechanical effect upon isotope effects, namely the energy quantization of bound modes of vibrations - frequently the principal component of isotope effects in reactions that behave classically. Another quantum behavior that influences all chemical reactions to varying degrees is quantum tunneling, which arises from the wavelike behavior that manifests in the unbound degrees of freedom. Tunneling is a quantum mechanical phenomenon involving penetration of the wave function for the molecule through the potential energy barrier of the reaction rather

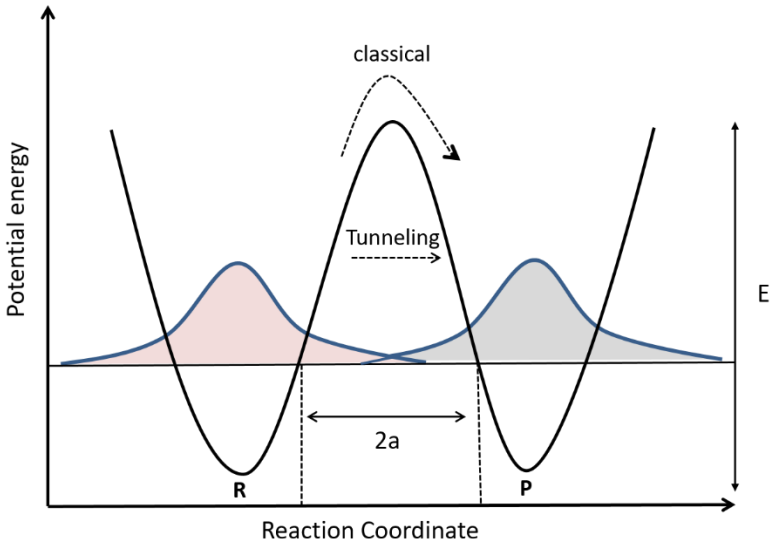

Figure 4. A figure demonstrating an example of ground-state nuclear tunneling along the reaction coordinate. "R" labels the reactant well and "P" labels the product well. E is the barrier height and 2a is the barrier width. The blue line represents the probability density function of a particle at the ground energy level. The area of the overlap region of reactant and product probability density functions denotes the probability of tunneling.[21]

than over it (Figure 4).[1] According to classical mechanics, a particle of mass *m* and energy *W* has to overcome the potential barrier (*W*>*E*) in order to transform reactant(s) into the product(s), and the probability of the reaction to take place is zero if *W* is less than *E*. According to quantum mechanics, however, the probability of a particle to appear on the product side is finite even when *W*<*E* and it increases gradually with increasing *W* and tends to unity when *W* tends to infinity.[22] The quantum mechanical solution of the transit probability or permeability *G* of a parabolic potential barrier with height *E* and width *2a* was obtained by Bell (*Equation 6*) using the WKB approximation.[23]

$$G(W) = \frac{1}{1+e^{\beta y}} \qquad \textit{Equation 6}$$

$$\beta = 2\pi^2 a(2mE)^{1/2} / h$$

$$y = 1 - W / E$$

As early as in 1933, Bell demonstrated that the tunneling effect is not negligible in some chemical reactions and recognized the necessity of quantum mechanical treatment for reactions - especially those involving the motion of light atoms like hydrogen.[22] In 1958, Bell[23] introduced a multiplicative correction factor Q_t to Eyring's[7] semiclassical rate constant expression (*Equation 7*), as shown in *Equation 8*. k_B is Boltzmann's constant, $\Delta G^{\ddagger}$ is

Gibbs free energy change from the reactant to the transition state, and $\nu^{\ddagger}$ is the imaginary frequency of the transition state.

$$k = \frac{k_B T}{h} \cdot e^{-\Delta G^{\ddagger}/RT} \qquad \textit{Equation 7}$$

$$k_{tunnel} = \boldsymbol{Q_t} \cdot \frac{k_B T}{h} \cdot e^{-\Delta G^{\ddagger}/RT} \qquad \textit{Equation 8}$$

$$Q_t \approx \frac{\frac{1}{2}u}{\sin\frac{1}{2}u} = 1 + \frac{u^2}{24} + \frac{7u^4}{5760} + \cdots, (u < 2\pi) \qquad \textit{Equation 9}$$

$$u = \frac{h\left|\nu^{\ddagger}\right|}{k_B T}, \qquad \nu^{\ddagger} = \frac{1}{2\pi} \cdot \sqrt{\frac{\partial^2 E}{m \cdot \partial x^2}}$$

Q_t is in the form of *Equation 9* only when u is less than 2π, which corresponds to $|\nu^{\ddagger}|$ less than $1000 cm^{-1}$ at room temperature. This is the case of most chemistry problems we are interested in. The first two terms in the expanded form of Q_t is identical to Wigner's correction that was derived at an earlier time. Since then, more sophisticated theories and computational methods have been developed and embedded in computer programs, one of which is called POLYRATE.[24]

1.4.2. The Phenomenological Manifestations of the Tunnel Effect

Since the development of the theories that predict tunneling effect on chemical kinetics, efforts have been made to the design and execute experiments capable of quantitatively testing these theories. The primary H/D KIE is the most useful experimental tool for investigating tunneling.[14] Several criteria for the diagnosing significant contributions from the tunnel effect have been determined from model calculations and justified by experimental results.[15,25-27] These criteria are summarized below:

(1) The magnitude of the KIE exceeds the semiclassical limit. The tunneling correction Q_t increases with increasing u according to *Equation 9*, which means Q_t increases with decreasing particle mass ($Q_{tH} > Q_{tD}$). Saunders proposed $k_H/k_D > 12$ at 25 °C to be a reasonable indication of tunneling (p. 141 in Ref.[15]). However, KIEs smaller than the maximum can contain contributions from tunneling as well. As discussed in section 1.3.1, KIEs are usually less than the maximum because of compensatory vibrations that develop at the TS. A small semiclassical KIE amplified by the tunnel effect can still be below the semiclassical limit.

(2) The plot of ln(k_H/k_D) vs. 1/T is nonlinear at low temperatures. The Arrhenius plot of the rate constant (ln(k) vs. 1/T) should be linear if the tunnel effect on the reaction rate is negligible (*Equation 10*). Tunneling is most important at low temperatures as Q_t

$$\ln(k) = \ln(A) - \frac{E_a}{R} \cdot \frac{1}{T} \qquad \textit{Equation 10}$$

$$\ln(k_H / k_D) = \ln(A_H / A_D) + \frac{E_{a,D} - E_{a,H}}{R} \cdot \frac{1}{T} \qquad \textit{Equation 11}$$

increases with decreasing temperature. The Arrhenius plot of rate constant should deviate from linearity and curve up at low temperatures (Figure 5A)[27]. As a result, ln(KIE) should violate the linear relationship with 1/T at lower temperatures, since the rate constant of H is more affected by tunneling than its heavier isotope D (Figure 5B). ln(KIE) is expected to plateau at very low temperatures, when tunneling affect H and D to the similar degree.

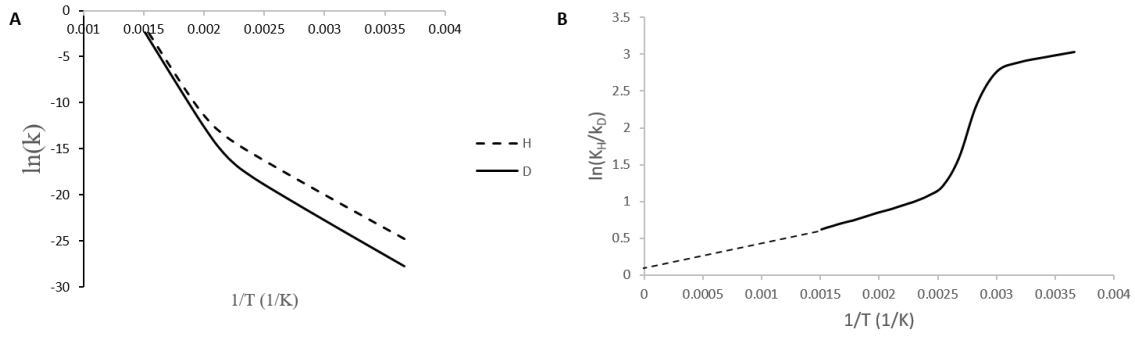

Figure 5.A) Arrhenius plot of rate constant of protium and deuterium. B) Arrhenius plot of KIE (k_H/k_D).

The Arrhenius pre-exponential factor ratio (A_H/A_D) is significantly greater than or less than unity. It was predicted by Bell (p. 88-90 in Ref.[25]) that A_H/A_D should be restricted to the range of 0.5-$\sqrt{2}$ and close to unity. The range was later refined by Stern and Weston[26] to 0.7-$\sqrt{2}$. This manifest can be understood with the illustration of Figure 5B and *Equation 11*. ln(A_H/A_D) is the y intercept of ln(k_H/k_D). At high temperatures, the KIE follows semiclassical TST and ln(k_H/k_D) intercept with y axis close to zero. At lower temperatures, the graph becomes steeper and should intercept with y axis at a lower value than 0.5 Figure 5B). At extremely low temperatures, the Arrhenius plot plateaus out and the y intercept is expected to be higher than the semiclassical limit $\sqrt{2}$. This criterion is sometimes more useful than criterion (2), because a curved Arrhenius plot can appear linear over a narrow temperature range.

(3) The rule of the geometric mean (RGM)[28,29] is violated. RGM predicts that the rate constant ratio between the protiated species to the double deuterated species should be the product of the KIE of the two singly deuterated species (*Equation 12*). The first

$$\frac{k_{HH}}{k_{DD}} = \frac{k_{HH}}{k_{DH}} \cdot \frac{k_{HH}}{k_{HD}} = 1^{\circ} KIE \times 2^{\circ} KIE \qquad \textit{Equation 12}$$

letter in the subscript of *k* stands for the atom that is being transferred and the second letter denotes the atom that is retained, so RGM is also an equation of 1°KIE and 2° KIE. In systems where tunneling effect is important, however, RGM is violated[30,31].

1.5. Traditional and New Experimental Methods for KIE Measurement

Measuring the kinetic isotope effect experimentally has become routine in chemistry and biology laboratories. The experimental design of determining the ratio of rate constants depends on the nature of the reaction to be studied (order of the reaction, fast or slow reaction), the positions of interest and the kind of information (rate-limiting step, product-limiting step, or the TS structure) to be extracted.

The standard and mostly applied types of experiments for KIE measurement[15,32] are summarized as method (A), (B) and (C). The methods are illustrated with hydrogen KIE, but are applicable on KIEs of other atoms.

(A) Non-competitive method

The rate constant for the light (e.g. H) and heavy (e.g. D) isotopomers can be measured

$$S_H \xrightarrow{k_H} P_H$$

$$S_D \xrightarrow{k_D} P_D$$

Figure 6. General schemes of two independent reactions of the same type but with different isotopomers as the starting material.

separately from two reaction runs in different containers by spectrophotometers (Figure 6). The KIE is then calculated from the ratio of the obtained rate constants (Equation 1). This method is straightforward, but the accuracy can be harmed by any inconsistency in the conditions (temperature, impurity, concentration etc.) between the two parallel reactions.

(B) **Intermolecular competition method**

Instead of running two separate reactions, the two isotopomers (e.g. protiated and deuterated) can be placed in the same container and react under exactly same the conditions. Based on the rate law, the rate constant ratio in this situation equals the ratio

of logarithm of one minus fractional conversion F (*Equation 13*). $[S_x]$ is the concentration of the starting material containing X isotope at fraction F_x, and $[S_x]_0$ is the initial concentration.

$$KIE_{inter} = \frac{k_H}{k_D} = \frac{\ln(\frac{[S_H]}{[S_H]_0})}{\ln(\frac{[S_D]}{[S_D]_0})} = \frac{\ln(1-F_H)}{\ln(1-F_D)} \qquad \textit{Equation 13}$$

$$KIE_{inter} = \frac{\ln(1-F_H)}{\ln[(1-F_H)\cdot R/R_0} \qquad \textit{Equation 14}$$

$$KIE_{inter} = \frac{\ln(1-F_H)}{\ln[1-(F_H R_p/R_0)]} \qquad \textit{Equation 15}$$

$$R = \frac{[S_D]}{[S_H]},\ R_0 = \frac{[S_D]_0}{[S_H]_0},\ R_p = \frac{[P_D]}{[P_H]}$$

Equation 13 can be rearranged into *Equation 14* and *Equation 15*. In such situation, no real time kinetic measurement is needed, only R_0, F_H, R or R_p are needed. R_0 and R are the initial and final molar ratio between the isotopic starting material respectively, and R_p is the ratio of the products, and these ratios can be directly measured by mass spectrometer or nuclear magnetic resonance (NMR). (p.95-100 in Ref.[15])

(C) Intramolecular competition method

The third method involves molecule that possesses more than one chemically equivalent positions, and some of these positions are labelled and some are unlabeled (p.93-94 in Ref.[15]). The reaction at the labelled position will compete with the reaction at the unlabeled position (Figure 7). The rate constant ratio can be easily determined from the ratio between the corresponding product during the reaction, and the percent conversion does not affect the result. It needs to be pointed out that the KIE calculated this way is not a pure primary KIE but is "contaminated" by a secondary KIE. More discussion on how to make this type of KIE more informative will be placed in the following text and Chapter 2.

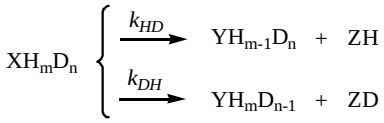

Figure 7.General scheme of intramolecular rate competition.[15]

$$KIE_{intra} = \frac{k_{HD}}{k_{DH}} = \frac{[ZH]}{[ZD]} = \frac{[YH_{m-1}D_n]}{[YH_mD_{n-1}]} \qquad \textit{Equation 16}$$

Shortcomings of the above traditional methods are:

(1) The above methods are only useful for the type of reaction that proceeds in a one single pathway. The KIE valued in the traditional ways can provide little useful mechanistic information if the reaction undergoes multiple pathways.

(2) Primary or secondary KIE cannot be measured directly by a single method in some cases. For example, considering a molecule that has two chemically equivalent hydrogen positions: i) If the position is fully labeled (double deuterated), the intermolecular competition between unlabeled (HH) versus fully labeled (DD) molecule will generate rate ratio of k_{HH}/k_{DD}, which is a composite KIE can equals 1° KIE×2 ° KIE (*Equation 12*). ii) If the position is partially labeled (singly deuterated), the intermolecular competition reactions between HH and HD will give a KIE which is a composite of the 1° KIE and 2 ° KIE. iii) If intramolecular competitive method is applied with partially labeled reactant, then as discussed in method (C) above, the resulting KIE is ratio of the primary KIE to the secondary KIE (1° KIE/2 ° KIE) as is illustrated in the experiments described in Chapter 2). Since the isolated primary and secondary KIEs are most useful for building reaction mechanism models, methods need to be develop in order to evaluate pure 1° KIE and 2° KIE instead of a composite KIE.

In order to maximize the utility of KIEs as an experimental observable, new KIE measurement methods have been developed and are described in method (D) and (E) below.

(D) Product specific intermolecular KIE

Xiang and Meyer[33] developed a method that allows one to evaluate the isotope effect on the rate constant of multiple reaction pathways (Figure 8). The KIE for product P_i that is formed through pathway i can be calculated from *Equation 17*, in which KIE_{inter} is standard intermolecular KIE that can be evaluated with *Equation 14*. Although this method was first demonstrated with the ^{13}C KIE of the cobalt mediated C-C bond formation between cyclopentene and 1-phenyl-1-propyne, it can be generalized to KIE measurement for other elements and for other multi-pathway reactions. Product-specific KIEs are unique in that they quantify fractionation that occurs in both product- and rate-determining steps.

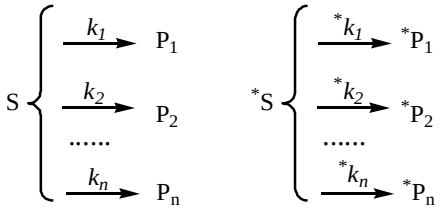

Figure 8. A general scheme of a reaction with multiple reaction pathways. Reactant S undergoes pathway i with rate constant k_i to produce product P_i (i=1, 2…n). The "" signifies the heavier isotope (e.g. D, ^{13}C, etc.).*

$$KIE(P_j) = KIE_{inter} \cdot \frac{(\sum_i^n [^*P_i]) / [^*P_j]}{(\sum_i^n [P_i]) / [P_j]} \qquad \textit{Equation 17}$$

(E) Combination of intramolecular and intermolecular measurement method

A method of isolating primary and secondary KIE from intermolecular and intramolecular KIE has been developed to resolve the shortcoming #2 of traditional methods. The new method adopts both intramolecular and intermolecular competitive experiments as shown in Figure 9. In the new method, KIE_{inter} is measured by method (B) and KIE_{intra} is measured by method (C).

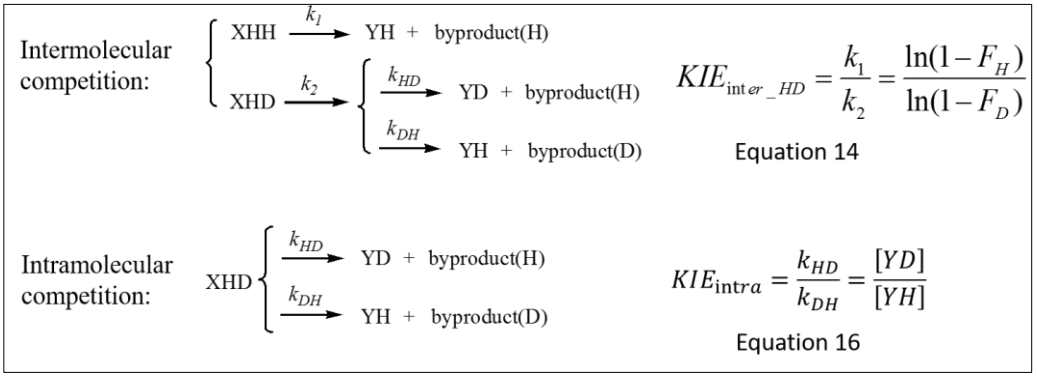

Figure 9. Intermolecular competition and intramolecular completion KIE measurements are combined to study a reaction.

According to the definitions, 1° and 2° KIE can be expressed as:

$$1^o\,KIE = \frac{k_{HH}}{k_{DH}} \qquad \textit{Equation 18}$$

$$2^{o}\,KIE = \frac{k_{HH}}{k_{HD}} \qquad \textit{Equation 19}$$

Dividing both sides of *Equation 18* by *Equation 19* gives:

$$KIE_{intra} = \frac{1^{o}\,KIE}{2^{o}\,KIE} \qquad \textit{Equation 20}$$

Examining the intermolecular competition scheme in Figure 9 closely, intermolecular can be expressed as follows:

$$KIE_{inter\_HD} = \frac{k_1}{k_2} = \frac{2k_{HH}}{k_{DH} + k_{HD}} \qquad \textit{Equation 21}$$

Dividing both the numerator and denominator of *Equation 21* by $k_{(HH)}$ and comparing with *Equation 18* and *Equation 19* gives:

$$KIE_{inter\_HD} = \frac{2}{\frac{k_{(DH)}}{k_{(HH)}} + \frac{k_{(HD)}}{k_{(DH)}}} = \frac{2}{\frac{1}{1^{o}\,KIE} + \frac{1}{2^{o}\,KIE}} \qquad \textit{Equation 22}$$

Solving *Equation 20* and *Equation 22* for 1° KIE and 2° KIE affords:

$$1°KIE = \frac{KIE_{Inter}\left(1 + KIE_{Intra}\right)}{2} \qquad \textit{Equation 23}$$

$$2°KIE = \frac{KIE_{Inter}\left(1 + 1/KIE_{Intra}\right)}{2} \qquad \textit{Equation 24}$$

The errors of primary and secondary KIE calculated this way are propagated as follow:

$$\Delta 1^{\circ}KIE = \frac{1}{2}\sqrt{\frac{\partial 1^{\circ}KIE}{\partial KIE_{\mathrm{int}\,er}}\cdot \Delta KIE_{\mathrm{int}\,er} + \frac{\partial 1^{\circ}KIE}{\partial KIE_{\mathrm{int}\,ra}}\cdot \Delta KIE_{\mathrm{int}\,ra}} \qquad \textit{Equation 25}$$

$$\Delta 2^{\circ}KIE = \frac{1}{2}\sqrt{\frac{\partial 2^{\circ}KIE}{\partial KIE_{\mathrm{int}\,er}}\cdot \Delta KIE_{\mathrm{int}\,er} + \frac{\partial 2^{\circ}KIE}{\partial KIE_{\mathrm{int}\,ra}}\cdot \Delta KIE_{\mathrm{int}\,ra}} \qquad \textit{Equation 26}$$

1° and 2° KIE can be calculated with *Equation 23* and *Equation 24*, for reactions whose primary and/or secondary KIE cannot be measured directly by one type of traditional KIE measurement experiment. Note that this method is only valid for reactions whose rate-determining step is the same as the product-determining step.

1.6.Computational Methods for Calculating Kinetic Isotope Effect

1.6.1. Bigeleisen Equation

Traditional computation of kinetic isotope effects is based on the theory of absolute reaction rates or transition state theory (TST) developed by Eyring et. al.[7] The expression for absolute reaction rate is often called Eyring equation and has a general form as shown in *Equation 7*. *Equation 7* can be written in equivalent but more detailed and computationally useful form as in *Equation 27* and *Equation 28*. The former is based on the thermodynamic relationship between free energy, enthalpy, and entropy: $\Delta G = \Delta H - T\Delta S$. The latter is based on statistical mechanics, where Q_R and $Q^{\ddagger}$ are the partition function, per unit volume, of the reactant R and of the transition structure with the decomposition mode excluded.[15] E_{class} is the classical molar heat of reaction that does not include the zero-point energy contribution. The partition function Q is the product of translational, rotational and vibrational partition functions ($Q=Q_{trans}Q_{rot}Q_{vib}$).

$$k = \frac{k_B T}{h}\cdot e^{-\Delta H^{\ddagger}/RT}\cdot e^{-\Delta S^{\ddagger}/R} \qquad \textit{Equation 27}$$

$$k = \frac{k_B T}{h}\cdot \frac{Q^{\ddagger}}{Q_R}\cdot e^{-E_{class}/RT} \qquad \textit{Equation 28}$$

The classical activation energy, E_{class}, is identical for different isotopologues or isotopomers, leading to a cancellation that yields the KIE as a compound ratio of partition functions corresponding to the reactant and transition structure species (*Equation 29*).

$$\frac{k_H}{k_D} = \frac{Q_H^{\ddagger}}{Q_D^{\ddagger}}\cdot \frac{Q_{R,D}}{Q_{R,H}} \qquad \textit{Equation 29}$$

Bigeleisen[34] derived an equation for KIE based on the transition state theory and the principle of quantum mechanical treatment of isotopic equilibria developed by himself and Mayer[35]. *Equation 30* is the most convenient expression of the Bigeleisen equation.[15]

$$KIE_{sc} = \left(\frac{k_H}{k_D}\right)_{sc} = \frac{\nu^{\ddagger}_{im,H}}{\nu^{\ddagger}_{im,D}} \cdot \prod_{i}^{3N^{\ddagger}-7} \left(\frac{u^{\ddagger}_{i,H}}{u^{\ddagger}_{i,D}} \cdot \frac{e^{\frac{u^{\ddagger}_{i,D}}{2}}}{e^{\frac{u^{\ddagger}_{i,H}}{2}}} \cdot \frac{1-e^{-u^{\ddagger}_{i,D}}}{1-e^{-u^{\ddagger}_{i,H}}}\right) \cdot \prod_{i}^{3N-6} \left(\frac{u_{i,D}}{u_{i,H}} \cdot \frac{e^{\frac{u_{i,H}}{2}}}{e^{\frac{u_{i,D}}{2}}} \cdot \frac{1-e^{-u_{i,H}}}{1-e^{-u_{i,D}}}\right) \qquad \textit{Equation 30}$$

$$u_i = \frac{h\nu_i}{k_B T}$$

KIEs can be conveniently calculated with the Bigeleisen equation by plugging in the normal mode frequencies of the transition state structure ($\nu_i^{\ddagger}$) and the reactant (ν_i) of the light and heavy isotopomers. frequencies can be easily obtained by normal mode frequency calculation of the optimized electronic molecular structure carried out by an electronic structure software package. All structures used in this dissertation were optimized using Gaussian 09[36].

The Bigeleisen equation treats the bound vibrations quantum mechanically and includes the effect of the ZPE, but the unbound imaginary vibrational mode is treated classically and no tunneling effect is considered, so the resulting KIE is called semiclassical KIE (KIE_{sc}). Tunneling can be included in the KIE calculation by multiplying the semiclassical KIE by the ratio of Bell's correction factor Q_t (*Equation 31*).

$$KIE_{tunnel} = \frac{Q_{t,H}}{Q_{t,D}} \cdot KIE_{sc} \qquad \textit{Equation 31}$$

1.6.2. POLYRATE

KIEs can also be calculated with the program - POLYRATE[24], which computes rate constant of not only the semiclassical transition state theory (TST) but also the canonical variational theory (CVT). The program also computes various types of tunneling corrections including the Wigner's correction (similar to Bell's correction, more information in section 1.4.1), zero-curvature tunneling (ZCT) correction, small curvature tunneling (SCT) correction and large curvature tunneling (LCT) correction.

POLYRATE can be used as a standalone program with an analytical potential energy surface (PES), but it is more widely used with GAUSSRATE[37] as the interface to Gaussian 09. GAUSSRATE contains codes that can call Gaussian to calculate the energies, gradients and Hessians at specific geometries when POLYRATE needs the information for the PES. Calculating the dynamic process directly from ab initio electronic structure properties like what GAUSSRATE does is called direct dynamics[38].

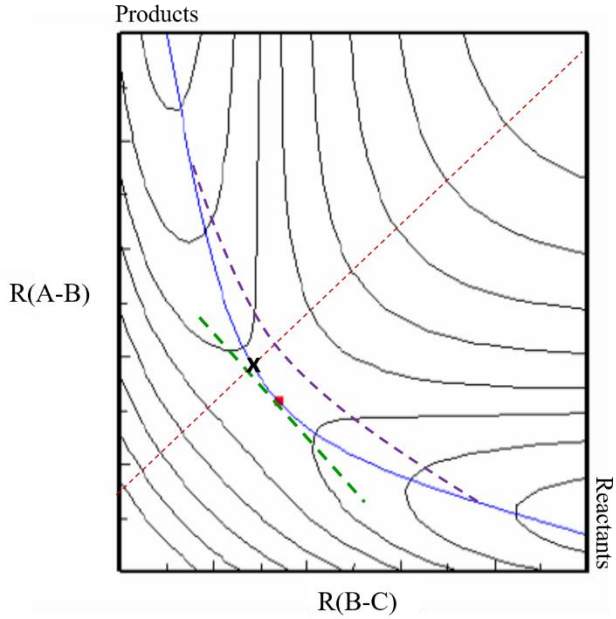

*Figure 10. The potential energy diagram for the collinear reaction AB+C → A+BC. The blue curve represents the MEP/ The red dot on the MEP denotes the saddle point. The dark red dashed line intercepting with the MEP at an **X** is a possible CVT dividing surface. The green dotted line is the approximated one-dimensional Wigner tunneling path and the purple dotted line is the multi-dimensional tunneling (SCT, TLC) path.*[39]

CVT: The canonical variational transition state theory (CVT or VTST)[40-42] is developed to improve the TST, whereby the dividing surface is positioned in such a way as to variationally minimize the rate constant. TST rate constant is calculated by evaluating the one-way flux of trajectories through the transition state in the product direction. In a multidimensional model of reaction potential energy surface, the transition state is a hypersurface (the dividing surface) that passes through the saddle point and is perpendicular to the minimum energy pathway (MEP) of the reaction. The error of TST is rooted in its assumption. The fundamental assumption of TST is the "dynamic bottleneck assumption" that assumes molecules passing the transition state all proceed to transform into the product and do not re-cross back to the reactant side. Thus, the rate constants predicted by TST is and upper bound of the true result because re-crossing does occur and diminish the rate. One way to improve TST is to vary the location of the dividing surface to minimized the rate constant.

The saddle point is the maximum along the reaction coordinate (s, the MEP) but a minimum in other dimensions on the potential energy surface (Figure 10). "s" is set to be 0 at the saddle point by conventional and also in POLYRATE. The potential energy (*V*) discussed here is classical and does not contain zero-point energy correction. The TST rate constant is calculated by plugging in V_{max} for E_{class} in *Equation 28*, as shown in

$$k^{TST}_{(s=0)} = \frac{k_B T}{h} \cdot \frac{Q^{\ddagger}}{Q_R} \cdot e^{-V_{\max}^{\ddagger}/RT} \qquad \textit{Equation 32}$$

$$V_{\max} = V\big|_{s=0}$$

$$k^{CVT}(s^{CVT},T)=\frac{k_BT}{h}\cdot\frac{Q^{\ddagger}}{Q_R}\cdot e^{-V\left|_{s^{CVT}}\right.^{\ddagger}/RT}=\frac{k_BT}{h}\cdot e^{-\Delta G_{\max}{}^{\ddagger}/RT}=\min_s k(T,s) \qquad \textit{Equation 33}$$

In CVT, the dividing surface is not constrained to include the saddle point, but is frequently shifted toward the reactant side or the product side depending on the result from maximizing the variational free energy of activation ΔG (Figure 10). The CVT rate constant (k^{CVT}) calculated at s^{CVT} where ΔG is at the maximum at a certain temperature is the minimum rate constant along the reaction coordinate (*Equation 33*).[41] V_{max} and ΔG_{max} are usually located at different s. As a result, CVT minimizes the re-crossing effect by finding the dynamical bottleneck.

The potential energy *V* reflects only the heat of the reaction and is indeed the enthalpy term. While the conventional TST consider only enthalpy in choosing the bottleneck, CVT also considers the entropic effects and zero-point energy effects associated with the $Q^{\ddagger}/Q_R$ term, so CVT should be, in principle, more accurate.[41]

SCT: Small curvature tunneling (SCT) correction in POLYRATE-version 2010 is based on centrifugal-dominant small-curvature semiclassical adiabatic ground-state (CD-SCSAG) method[41,43-45]. While Wigner correction includes only the tunneling effect from the imaginary vibration mode at the saddle point, SCT choose a curved reaction path in the classically forbidden region and includes the coupling between the reaction-coordinate motion with multiple other bound vibrational modes[46] (Figure 10). The corner cutting reaction path results in a thinner energy barrier and a larger transmission probability. SCT correction on the CVT rate constant has been shown to generate more accurate results than one-dimensional tunneling correction.[12,45]

Chapter 2. Mechanistic Study of the Chugaev Elimination

2.1 Mechanistic Background and Synthetic Utility of the Chugaev Elimination

The Chugaev elimination is an intramolecular syn-β-elimination reaction that forms olefins from the corresponding xanthate esters [ROC(S)SR']. The mechanism of the Chugaev elimination is well established. During the course of the reaction, the double-bonded sulfur of the xanthate abstracts one β-hydrogen atom via a six-membered cyclic transition state; a double bond is then formed in a concerted hydrogen removal and carbon-oxygen bond breakage step; the by-product rapidly decomposes to carbonyl sulfide (O=C=S) and methanethiol (CH_3SH) (Figure 11)[47,48].

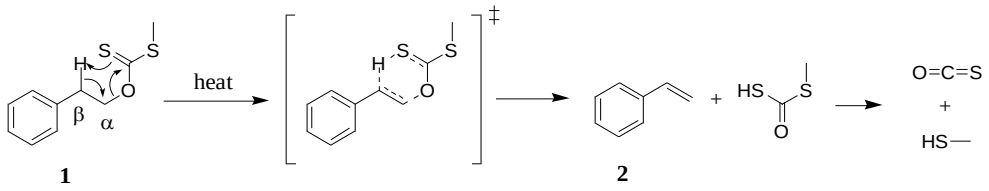

*Figure 11. Chugaev elimination reaction mechanism, using the elimination of S-methyl O-(2-phenyl) ethyl xanthate (**1**) as an example*

The Chugaev elimination is a simple yet useful conversion in synthetic chemistry. The reaction has been frequently adopted in the key synthetic routes to many natural and pharmaceutical products to transform alcohols to the corresponding olefins.[49-53] The Chugaev elimination is advantageous in that the byproducts are gaseous, which makes workup and purification negligible in most cases. Furthermore, the Chugaev elimination is a valuable model for mechanistic study because it is serves as a comparison with the Swern Oxidation where the intramolecular H/D KIE exhibits features that indicate that tunneling is important, although the observed KIE is minute even at low temperatures.[48] The Chugaev elimination serves as a contrast

In the project that will be elaborated in this chapter, the kinetic isotope effect of transferring the β-hydrogen atom in the Chugaev elimination of S-methyl O-(2-phenyl) ethyl xanthate (**1**) along with its various para-substituted analogs has been studied carefully. Conclusions about tunneling effect in the reactions will be drawn based on both experimental and computational results.

2.2. Methods

2.2.1. Intramolecular KIE Measurement

The intramolecular KIEs were measured according to method **(C)** described in section 1.5 by quantifying the isotopic product (**2** and d_1-**2**) distribution of the elimination of mono-deuterated S-methyl O-(2-phenyl) ethyl xanthate (d_1-**1**) (Figure 12). The KIE was calculated with *Equation 16*. In this case, $KIE_{intra}=[d_1\text{-}\mathbf{2}]/[\mathbf{2}]$.

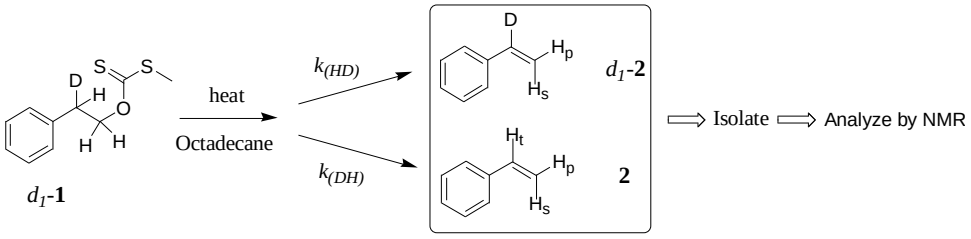

*Figure 12. The method for measuring intramolecular ^2H KIE at the benzylic position of d_1-**1**.*

In order to explore the temperature dependence of the intramolecular KIE, the measurement was carried out at eight different temperatures: 180℃, 190℃, 200℃, 210℃, 230℃, 250℃, 270℃ and 290℃.The product ratio was determined using quantitative ^1H NMR (peak H_t vs. peak H_s). Five replicate experiment were performed for each temperature. The final result was obtained by averaging among the five replicas. The same procedure was followed for measuring the intramolecular KIE of other para-substituted substrates.

2.1.2. Intermolecular KIE Measurement

The HH/HD intermolecular KIE ($KIE_{\_inter\_HD}$) was measured by running competition reactions between protiated xanthate (**1**) and mono-deuterated xanthate (d_1-**1**) to 40~50% conversion, and then by analyzing the reaction mixture and the re-isolated reactant (Figure 13). The KIE was calculated with *Equation 13* in section 1.5 method **(B)**. In this specific

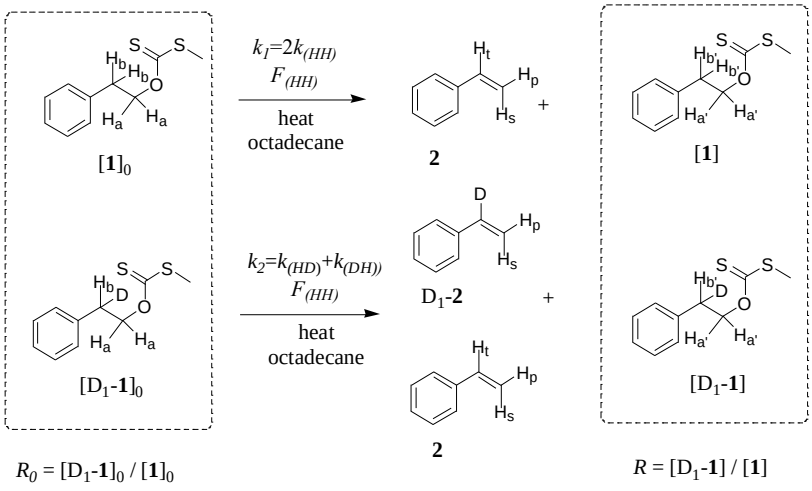

Figure 13. The method for measuring HH/HD intermolecular ^2H KIE.

experiment, the KIE is expressed in *Equation 34*. The percent conversion was determined by comparing the ^{1}H NMR peak integration between the product (H_p and H_s) and the re-isolated reactants ($H_{a'}$); and the isotopic fractionation was determined by integrating peak H_a, H_b, $H_{a'}$ and $H_{b'}$.

$$KIE_{inter\_HD} = \frac{k_1}{k_2} = \frac{\ln(1-F_{(HH)})}{\ln(1-F_{(HD)})} \qquad \textit{Equation 34}$$

where

$$1- F_{(HH)} = \frac{(1-F)(1+R_0)}{1+R} \quad \text{and} \quad 1- F_{(HD)} = \frac{(1-F)(1+\frac{1}{R_0})}{1+\frac{1}{R}}$$

The HH vs. DD inter-molecular KIE ($KIE_{\_inter\_DD}$) was measured by the same method. The equation for $KIE_{\_inter\_DD}$ is *Equation 35*.

$$KIE_{inter\_DD} = \frac{k_1}{k_2} = \frac{\ln(1-F_{(HH)})}{\ln(1-F_{(DD)})} \qquad \textit{Equation 35}$$

2.1.3. Primary and Secondary KIE Calculations

It is not possible to measure 1° nor 2° KIE directly by measuring intra or inter molecular KIE for the Chugaev elimination of **1**, because the two benzylic hydrogen atoms of **1** are chemically equivalent and cannot be distinguished by the sulfur atom that abstracts them. Fortunately, Chugaev elimination is a concerted one-step reaction and its rate- and product determining step is the same. In such systems, primary and secondary KIE can be calculated from intramolecular and intermolecular KIE based on method (E) in section 1.5.

2.1.4. Computational Methods

The computational KIE was calculated from the rate constants computed by running direct dynamics with GAUSSRATE[37] as the interface between POLYRATE[24] and Gaussian 09[36]. The geometry optimization, gradient and hessian calculations along the MEP were performed using M06-2X functional, 6-31+G(d,p) basis set and SMD solvent model for heptane.

The transition state is localized using both TST and CVT theories, and quantum tunneling effects were calculated with SCT (described in section 1.6.2). Rate constant was calculated for each of the isotopologs (Figure 14): $k_{(HH)}$, $k_{(DH)}$ and $k_{(HD)}$. The direct dynamic calculations were done in the reaction coordinate range of $-1 < s < 1$, at which range the tunneling properties were found to converge.

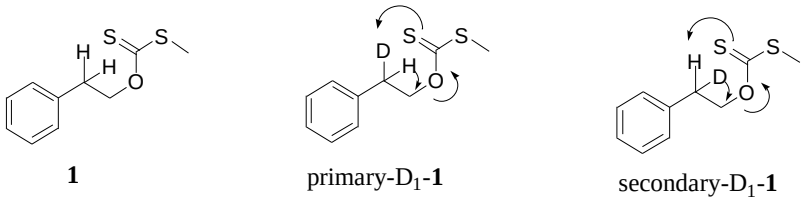

*Figure 14. Three isotopologs of **1** for POLYRATE calculations*[54]

2.3. Results and Discussion

2.3.1. Temperature Dependence of ^{2}H KIEs

The temperature dependence of intramolecular KIE for Chugaev elimination was examined over the temperature range from 180 °C to 290 °C. Based the experimental and computational data (Figure 15), there are three major informative observations. First, the Arrhenius pre-exponential factor A_{HD}/A_{DH} obtained from the linear fit of the experimental data is well within the semiclassical limit. The A_{HD}/A_{DH} obtained is 0.76, and the semiclassical range is 0.7 to 1.4. Second, the experimental data possess a concave-upward Arrhenius relationship, which is indicative of tunneling. However, this evidence is not invulnerable because the degree of curvature is so small. Third, the experimental data are smaller than those predicted by semiclassical TST especially at high temperatures. This observation is contrary to what is frequently observed, since semiclassical TST with no tunneling correction typically generate KIE lower than the experimental values even in case where tunneling is thought to have the smallest influence[55].

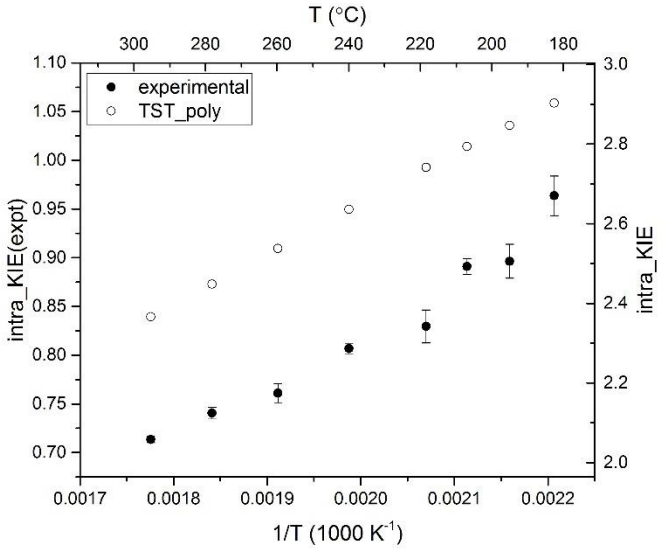

Figure 15. The Arrhenius plots of intramolecular H/D KIE measured from experiments and computed by POLYRATE at transition state theory (TST) level. The KIE values are also tabulated in **Table 1**.

The intramolecular KIE results of the Chugaev elimination provide ambiguous evidence for tunneling, which is not dissimilar to other syn-β-elimination reactions. About thirty years ago, Harold Kwart studied the temperature dependence of the intramolecular KIEs of a series of syn-β-eliminations and generated linear Arrhenius relationship in all the systems he studied[56-58]. Many of the intramolecular KIE Kwart observed were of low magnitude even in systems where tunneling plays a significant role (e.g. $k_{HD}/k_{HD}=A_{HD}/A_{HD}=2.2$ for amine oxide thermolysis from 90°C to 210°C[56]). Recent work by Giagou and Meyer on Swern oxidation of benzyl alcohol observed a concave-up Arrhenius plot with abnormally small intramolecular KIE (2.53 at -78 °C)[8].

Intramolecular KIE can be expressed as the ratio of primary and secondary KIE as shown in *Equation 20*, so the low magnitude of intramolecular KIE can be attributed to an abnormally low primary KIE or an abnormally high secondary KIE. In order to examine primary and secondary KIE separately instead of as a ratio, intermolecular KIEs were measured by running competition reaction between protiated- and mono-deuterated-xanthate (results are in **Table 1**).

Table 1. Intramolecular and intermolecular KIE of the Chugaev elimination. *

T (°C)	KIE_{intra}	KIE_{intra} (TST_POLYRATE)	KIE_{inter} **HH vs. HD**	KIE_{inter} **HH vs. DD**
180	2.62±0.05	2.88	2.49±0.08	--
190	2.45±0.04	2.82	2.13±0.15	6.64±0.12
200	2.44±0.02	2.76	1.96±0.19	--
210	2.29±0.04	2.70	1.86±0.09	--
230	2.24±0.01	2.59	1.73±0.06	--
250	2.14±0.02	2.48	1.56±0.07	--
270	2.10±0.01	2.39	1.55±0.04	--
290	2.04±0.01	2.32	--	--

*Data are experimental results otherwise stated.

The primary and secondary KIEs calculated from the experimental intramolecular and intermolecular KIEs both possess concave-up Arrhenius plots (Figure 16). By comparing the experimental KIEs with those predicted by TST, it can be found that transition state theory approximates the primary KIE better than the secondary KIE, and the secondary KIE is underestimated much by TST (Figure 16). This means that the secondary KIE that occurs at a position where no hydrogen atom transfer from the donor to the acceptor occurs is more amplified by tunneling effect than is the primary KIE when compared to the semiclassical TST KIE values ($Q_{t(expt.)}$ 2° > $Q_{t(expt.)}$ 1°) as shown in **Table *2***. The magnitude of the secondary KIEs at low temperatures are found to be exceptionally big. The secondary KIE at 180 °C is 1.72 and is the largest secondary KIE measured to our knowledge. The intermolecular KIE between protiated and dideuterated xanthates (HH vs. DD) serves as another evidence of intensive tunneling. According to the rule of the geometric mean (RGM), k_{HH}/k_{DD} should be the product of 1° and 2° KIE (section 1.4.2). At 190 °C, 1° KIE × 2° KIE = 3.67× 1.50 = 5.505 (**Table *2***). This value is smaller than the dideuterated

intermolecular KIE ($KIE_{\_inter(HH\ vs.\ DD)}$, **Table 1**), indicating a great tunneling factor in the reaction.

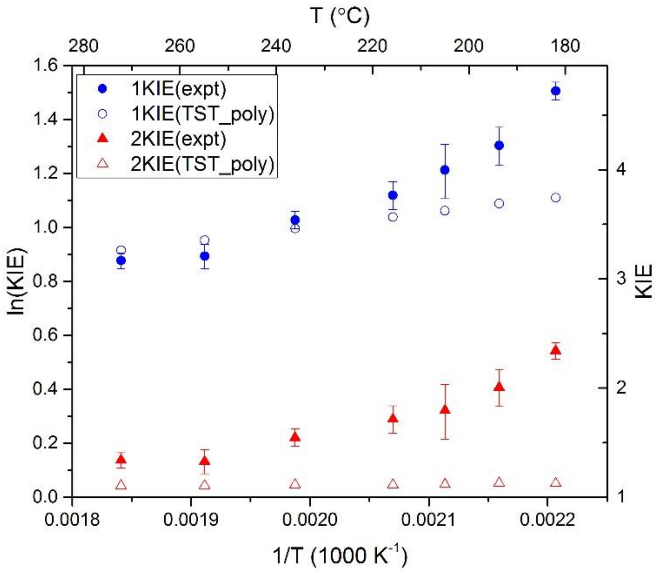

Figure 16. The Arrhenius plots of primary and secondary KIE of Chugaev elimination obtained from experiments and POLYRATE calculation of TST rate constants with M06-2X/6-31+G(d,p) functional/basis set.

The abnormally inflated magnitude of the 2° KIE is not predicted by the one-dimensional tunneling model, which predicts that tunneling affects the atom being transferred the most. Our findings imply the significance of tunneling effect not only for the atom that is being transferred but also for other atoms. This observation is not surprising if the saddle point's vibrational modes are examined. Although the hydrogen atom that remains on the α carbon is not transferred from a donor to an acceptor, it undergoes rehybridization from the sp^3 to sp^2 state, which can be considered as a certain mode of motion Figure 17. Such

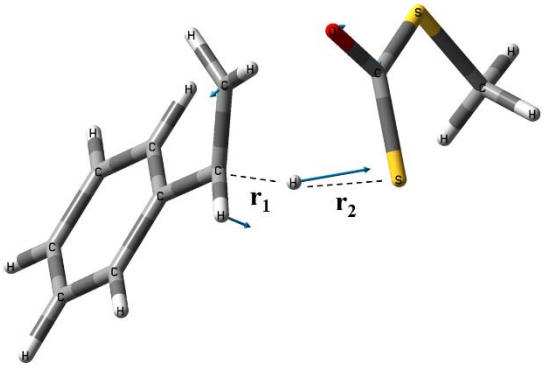

Figure 17. The saddle point structure for the Chugaev elimination. The blue arrows represent the displacement vectors of the imaginary vibrational mode. r_1 is the distant between the α-carbon and the transferred hydrogen and r_2 is the distance between the transferred hydrogen and the double bonded sulfur.

motion of the hydrogen at the "secondary" position also exhibit quantum behavior. This hypothesis is not evoked for the first time. It was proposed by Saunders in a model calculation research work in 1984.[59]

Table 2. Experimental and computational primary and secondary KIEs for Chugaev elimination.

T(°C)	expt. [a]	TST [b]	CVT [b]	CVT/SCT[b]	k^{TST}/k^{CVT}	$Q_{t\ (expt.)}$ [c]	$Q_{t\ (CVT/SCT)}$ [d]	$Q_{t\ (Bell)}$ [e]
	1° KIE							
180	4.51±0.15	3.03	2.22	2.58	1.36	1.486	1.138	1.127
190	3.67±0.25	2.97	2.19	2.52	1.36	1.236	1.134	1.120
200	3.36±0.34	2.89	2.15	2.46	1.35	1.163	1.131	1.114
210	3.06±0.16	2.83	2.11	2.41	1.34	1.083	1.128	1.109
230	2.80±0.09	2.71	2.04	2.33	1.33	1.032	1.123	1.099
250	2.44±0.11	2.59	1.98	2.24	1.31	0.943	1.119	1.090
270	2.40±0.07	2.50	1.92	2.17	1.30	0.963	1.116	1.083
	2° KIE							
180	1.72±0.05	1.05	1.11	1.13	0.95	1.635	1.018	1.0230
190	1.50±0.10	1.05	1.11	1.12	0.95	1.421	1.016	1.0218
200	1.38±0.14	1.05	1.11	1.12	0.95	1.315	1.015	1.0207
210	1.34±0.07	1.05	1.11	1.12	0.95	1.276	1.015	1.0198
230	1.25±0.04	1.05	1.11	1.12	0.95	1.191	1.013	1.0180
250	1.14±0.05	1.04	1.11	1.11	0.94	1.094	1.012	1.0164
270	1.15±0.03	1.04	1.10	1.11	0.95	1.099	1.011	1.0151

[a] Data calculated from experimental KIE_{intra} and $KIE_{inter.}$ [b] Data calculated from POLYRATE output. [c] $Q_{t\ (expt.)}$ =KIE(expt.) / KIE(TST). [d] $Q_{t\ (CVT/SCT)} = \kappa^{CVT/CAG} \times \kappa^{SCT}$ (κ values are from POLYRATE output; $\kappa^{CVT/CAG}$ is the transmission coefficient at CVT level of theory, and κ^{SCT} is the small curvature tunneling transmission coefficient.) [e] $Q_{t\ (Bell)}$ is calculated with *Equation 9*.

To seek theoretical model to quantitatively explain our experimental data, POLYRATE calculations were carried out. Canonical variational transition state theory (CVT) was used to calculate KIEs and was found to approximate the secondary KIE better than TST did. As **Table 2** shows, CVT elevates 2° KIEs and lowers 1° KIE relative to TST. The variationally optimized transition structures of the Chugaev elimination were found to be shifted to the product side on the reaction coordinate (Figure 18). The CVT transition state

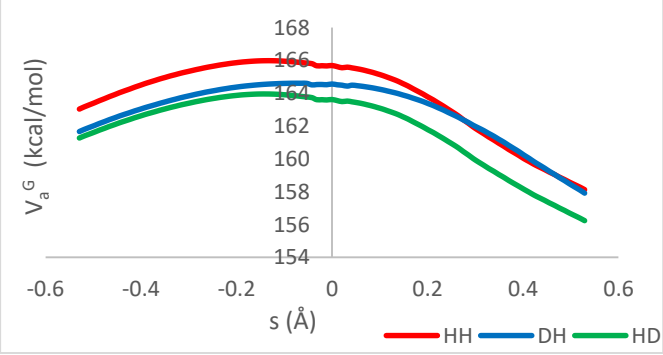

Figure 18. Adiabatic ground-state energy (V_a^G) diagram for HH, DH and HD reaction species. The reaction coordinate "s" is in mass-scaled angstrom. $V_a^G = V_{(MEP)}$ + ZPE.

is located 0.137 Å away from the saddle point for HH species (from naturally abundant reactant), 0.121 Å for DH species (the deuterated hydrogen is transferred) and 0.146 Å for HD species (the deuterated hydrogen is retained) at 180 °C (**Table 3**). Small curvature tunneling (SCT) and Bell's correction factors were calculated to approximate the tunneling effect (**Table 2**), but none of the methods seems to reproduce the experimental results. A previous publication states that quantum correction is important for calculating the absolute rate constant and variationally optimized bottleneck location is important for calculation KIE.[60]

Table 3. Bottleneck properties of the Chugaev elimination.

	HH			DH			HD		
	s (Å)[a]	r_1 (Å)	r_2 (Å)	s (Å)[a]	r_1 (Å)	r_2 (Å)	s (Å)[a]	r_1 (Å)	r_2 (Å)
Saddle Point	0	1.27	1.79	the same as HH			the same as HH		
CVT at 180 °C	-0.137	1.24	1.78	-0.121	1.24	1.48	-0.146	1.21	1.82
CVT at 290 °C	-0.139	1.21	1.82	-0.134	1.21	1.82	-0.149	1.21	1.82

[a] Reaction coordinate "s" is reported in mass-scaled angstrom.

2.3.2. Effects of Driving Force upon ^{2}H KIEs

The intramolecular KIE for the xanthates with the electron donating group methoxy group (-OMe) and the electron withdrawing group nitro group (-NO_2) at the para position on the benzene ring possess similar temperature dependence as does the unsubstituted (H at the para position) xanthate. The Arrhenius plots of the reaction with -OMe and -NO_2 substituents are linear (Figure 19).

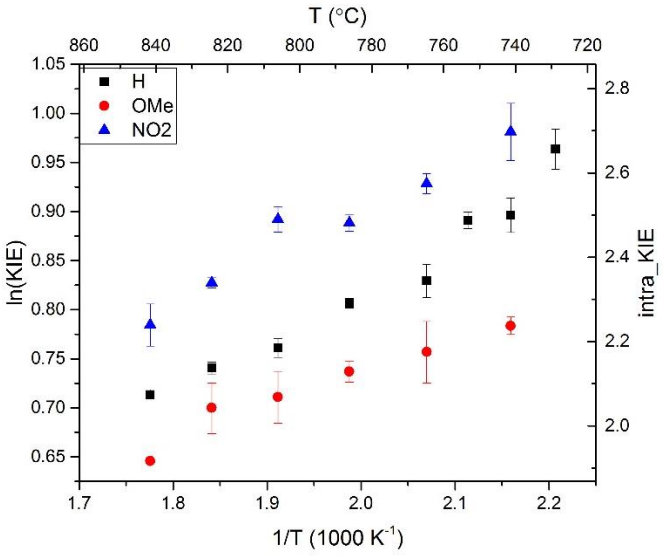

Figure 19. The Arrhenius plots of intramolecular KIE for H, methoxy (OMe) and nitro (NO_2) substituted xanthates.

The linear free energy relationship (LFER) was studied for Chugaev elimination with five different substituents (-OMe, -Me, -H, -Cl, -NO_2). The natural logarithm of intramolecular KIEs were plotted over the substituent parameter σ_{para} (Figure 20). The plots shown are similar to Hammett plots that plot the natural logarithm of the ratio between rate constant of substituent X and that the reference substitient H (k_X/k_H) over Hammett parameters (σ values).[61] Recent research by Sigman and co-workers shows that structure-activity relationship can also be efficiently studied by correlating the various types of reaction-related properties (reaction rate, KIE, enantioselectivity etc.) to the structure-related parameters (Hammett electronic parameters, Taft steric parameters[62] etc.).[6,63,64]

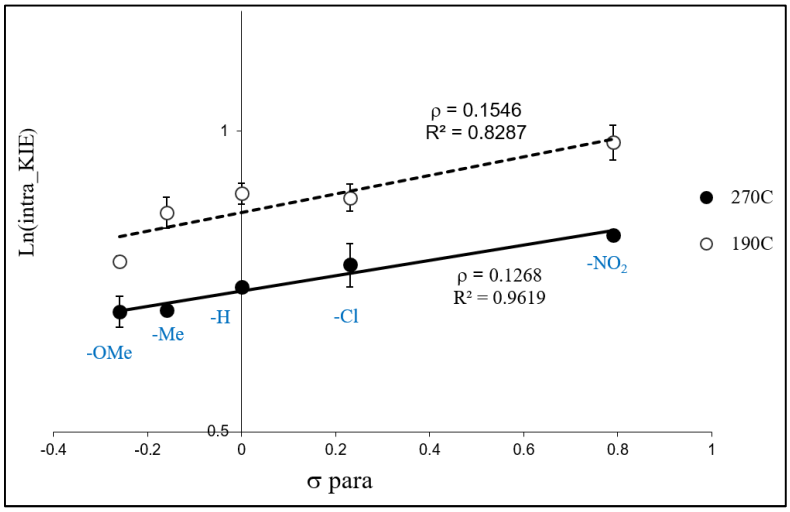

Figure 20. Plots of natural logarithm of intramolecular KIE of Chugaev elimination vs σ_{para} values at 190 °C and 270 °C.

The free-energy linear correlation of the intramolecular KIEs to σ_{para} is excellent at the higher temperature (270 °C) but poor at the lower temperature (190 °C) (Figure 20). As the temperature dependency of 1° and 2° KIEs shows, the Chugaev elimination is more affected by tunneling effect at 190 °C than at 270 °C. This indicates that tunneling makes the Hammett-type plot deviate from linearity. Another feature of the free-energy relationship of Chugaev elimination is the small magnitude of the ρ values (0.13 at 270 °C and 0.15 at 190 °C), meaning the KIEs for the reaction do not depend strongly on the substituents.

Figure 21 shows the free-energy correlation of intermolecular, 1° and 2° KIEs to σ_{para} is poor at 190 °C ($R^2 \approx 0.2$). This observation is expected and is consistent with the first conclusion drawn for LFER of the intramolecular KIE, because great tunneling effect is reflected in the intermolecular, 1° and 2° KIEs at 190 °C.

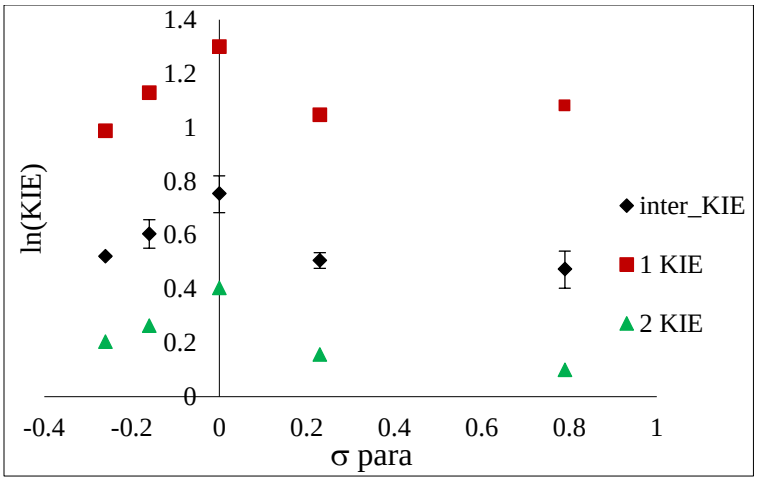

Figure 21. Plots of natural logarithm of intermolecular, 1° and 2° KIEs of Chugaev elimination vs σ_{para} values at 190 °C

2.4. Conclusion

This chapter explored the hydrogen transfer mechanism of Chugaev elimination using a combined experimental and computational approach. The former include the combination of intramolecular and intermolecular KIE measurement along with LFER studies. Several insightful conclusions can be drawn from this work.

First, this chapter demonstrates the utility of a new method of extracting primary and secondary KIEs from experimental determinations of intramolecular and intermolecular KIEs in systems where primary and secondary KIEs cannot be measured directly. This new method enables the exploration of physical phenomena, including the multi-dimensional nature inherent to tunneling with appreciable curvature. This approach to extracting primary and secondary KIEs as an experimental observables appropriate to C–H functionalization at methylene groups demonstrates promise in elucidating the roles of physical phenomena in hydrogen transfer reactions.

Second, quantum tunneling is found to affect both primary and secondary KIE of Chugaev elimination according to their concave-up Arrhenius plots, but amplifies the secondary KIE more than the primary KIE. The exceedingly inflated secondary KIE accounts for the suppressed intramolecular KIE and is a result of the motion of the non-transfered hydrogen in the transition state. The trend in the experimental KIEs can be approximated by CVT calculation to a moderate degree, implying that the location of the dynamic bottleneck is dependent on isotopic substitution. Variational effects are important in determining the KIE. While POLYRATE results reproduce some of the observed trends in the experimental KIEs, none of the models for tunneling within POLYRATE reproduce the trends in a quantitative fashion. One-dimensional tunnel corrections also fail. The experimental data included in this chapter demonstrate a need for a more robust model for hydrogen tunneling.

Finally, LFER studies show that the concerted cyclic hydrogen transfer process in the Chugaev elimination has shallow dependence on the substituent, indicating the transition state structure is not influenced much by the electronic property of the benzene ring. It is also shown that tunneling effect interrupts the linearity of the relationship between free-energy and the Hammett parameter.

2.5. Experimental Section

Chemicals: styrene (Sigma-Aldrich), styrene-a-d_1 (Sigma-Aldrich), 4-methoxystyrene (Acros Organics), 4-methylstyrene (TCI), 4-Chlorostyrene (Acros Organics), 4-nitrobenzaldehyde (Sigma-Aldrich), 4-(trifluoromethyl)benzaldehyde (Sigma- Aldrich), sodium borohydride (Sigma-Aldrich), sodium borodeuteride (Sigma-Aldrich), iodine (Sigma-Aldrich), 30% hydrogen peroxide solution (Fischer Scientific), sodium hydroxide (Sigma-Aldrich), sodium hydride (Sigma-Aldrich), carbon disulfide (Sigma-Aldrich), iodomethane (Sigma-Aldrich), acetic acid (Sigma-Aldrich), sodium chloride (Fischer Scientific), magnesium sulfate(Fischer Scientific), triphenylphosphine (Sigma-Aldrich), potassium carbonate (Sigma-Aldrich), tetrahydrofuran (THF) (anhydrous, Acros Organics), octadecane (Acros Organics), pentane (Fischer Scientific), diethyl ether (Fischer Scientific), chloroform-d (Sigma-Aldrich), 5Å molecular sieves (Fischer), silica gel (40-63 mm, SORBTECH), deionized water (from household deionizer)

General: All reagents were commercially obtained otherwise noted. All reactions were carried out in flame-dried glassware and under nitrogen atmosphere. 5Å molecular sieves were activated by heating under the vacuum and were saved in sealed round bottom flask for no longer than one week prior to use. Moisture-sensitive liquids (e.g. THF) were dried over activated 5Å molecular sieves for at least 24 hours. Gastight syringe or stainless steel cannula were used to transfer air- and moisture- sensitive liquids. Column chromatography was performed with silica gel (particle size 40-63 μm) under reported solvent condition. In temperature controlled reaction experiments, the temperature was regulated by J-KEM, Model 210 thermo-controller (with thermocouple type J). Proton and deuterium nuclear magnetic resonance (^{1}H NMR and ^{2}H NMR) spectra were obtained on Varian 400 MR NMR spectrometer (400 MHz) or Agilent ProPulse 500 MHz NMR spectrometer. The NMR data are reported as follows: chemical shifts (δ) in ppm, multiplicity (s=singlet, d=doublet, t=triplet, dd=doublet of doublets, tt=triplet of triplets, m=multiplet, br=broad), integration.

2.5.1. Material Preparation

a. General procedure for synthesizing substituted styrenes

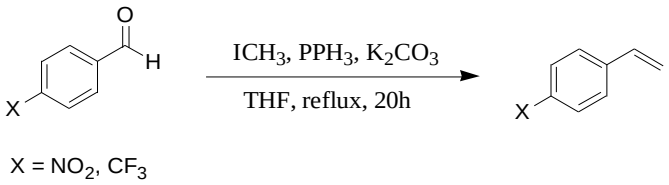

Figure 22. The reaction scheme of the synthesis of substituted styrene

In a 500ml 3-neck round bottom flask (RBF) that was equipped with an additional funnel and a condenser 350ml anhydrous THF was added. Triphenylphosphine (25g, 95.3mmol, 1.5 equiv.) and iodomethane (6ml, 13.68g, 96.4mmol, 1.5 equiv.) were added in to the RBF and stirred for 10 minutes. Potassium carbonate (27g, 195.3mmol, 3 equiv.) was added into the reaction mixture and stirred for 10 minutes, followed by addition of the corresponding para-substituted benzaldehyde (66.2mmol). The reaction mixture was refluxed for 20 hours. The cooled reaction mixture was mixed 500ml water. The mixture was stirred rigorously and extracted with 2×350ml ethyl ether. The organic layer was washed with 500ml saturated sodium chloride solution and dried with magnesium sulfate. The isolated product was purified by flash column chromatography under the conditions given bellow:

4-nitrostyrene: Purified by chromatography on silica gel (95:5 pentane: ethyl), colorless liquid; ^{1}H NMR ($CDCl_3$, 400MHz) δ: 5.46(d, 1H), 5.9(d, 1H), 6.7-6.8(dd, 1H), 7.5(d, 2H), 8.2(d, 2H).

4-(trifluoromethyl)styrene: Purified by chromatography on silica gel (95:5 pentane: ethyl), colorless liquid; ^{1}H NMR ($CDCl_3$, 400MHz) δ: 5.3(d, 1H), 5.78(d, 1H), 6.6-6.7(dd, 1H), 7.4 (d, 2H), 7.5 (d, 2H).

(Note: 4-ntirostyrene and 4-(trifluoromethyl)styrene were synthesized from the corresponding benzaldehyde via Wittig reaction due to the relatively high price of these two types of styrene. Other substituted styrenes were obtained commercially.)

b. General procedure for synthesizing 2-phenylethanols[65]

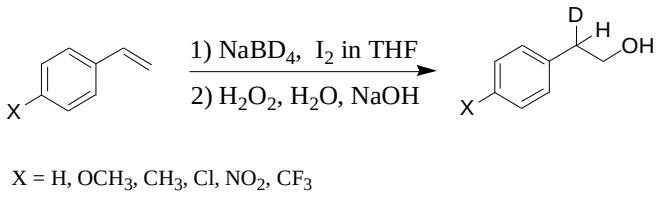

Figure 23. The reaction scheme for the synthesis of 2-phenylethanols

200 ml anhydrous THF was added into a dry, 500ml, 3-neck RBF (round bottom flask) which is equipped with an egg-shaped stir bar and a pressure-equilibrated addition funnel. 120ml THF was added to the additional funnel. Sodium borodeuteride (57.6 mmol, 0.5

equiv.) was added into in the RBF and allowed to dissolve in THF by stirring. Iodine (23 mmol, 0.2 equiv.) was added into the addition funnel and allowed to dissolve in THF by gently swirling. The iodine solution was added into the RBF drop-wise over 1.5 hour in ice bath. The corresponding styrene (115.2 mmol) was added slowly into the RBF. The reaction mixture was warmed up to room temperature while being stirred for 2 hours. 100ml 30% hydrogen peroxide solution and 100ml 3M sodium hydroxide solution was mixed. The resulting mixture was added into the reaction flask slowly with caution over ice bath. The mixture was then extracted with 3×200ml ethyl ether. The combined organic layers were washed with 500ml saturated sodium chloride solution, dried with magnesium sulfate and followed by removal of the solvent by rotary evaporation under reduced pressure. The crude product was purified by flash silica gel column chromatography under conditions given bellow.

***d_1*-2-phenylethanol:** Purified by chromatography on silica gel (3:1 pentane: ethyl ether), clear liquid (55%); ^{1}H NMR ($CDCl_3$, 400MHz) δ: 1.85 (broad s, 1H), 2.8 (tt, 1H), 3.85 (d, 2H), 7.0-7.4 (m, 5H).

***d_2*-2-phenylethanol:** The general procedure was followed, except that styrene-α-d_1 is used as the reactant instead of regular styrene. The product is purified on silica gel (3:1 pentane: ethyl ether), clear liquid (77%). ^{1}H NMR ($CDCl_3$, 400MHz) δ: 1.85 (broad s, 1H), 3.83 (d, 2H), 7.0-7.4 (m, 5H).

2-phenylethanol: The general procedure was followed, except that sodium borohydride was used instead of sodium borodeuteride. The product is purified on silica gel (3:1 pentane: ethyl ether), clear liquid (77%); ^{1}H NMR ($CDCl_3$, 400MHz) δ: 1.85 (broad s, 1H), 2.8 (t, 2H), 3.85 (t, 2H), 7.0-7.4 (m, 5H).

***d_1*-2-(4-methoxyphenyl) ethanol**: Purified by chromatography on silica gel (55:45 pentane: ethyl ether), clear liquid (61%); ^{1}H NMR ($CDCl_3$, 400MHz) δ: 1.85 (s, 1H), 2.8(tt, 1H), 3.75 (s, 3H) 3.8(d, 2H), 6.85 (d, 2H), 7.1 (d, 2H).

***d_1*-2-(4-methylphenyl) ethanol:** Purified by chromatography on silica gel (1:1 pentane: ethyl ether), clear liquid (65%); ^{1}H NMR ($CDCl_3$, 400MHz) δ: 1.85 (s, 1H), 2.3 (s, 3H), 2.8(tt, 1H), 3.85(d, 2H), 7.0-7.2 (m, 4H).

***d_1*-2-(4-chlorolphenyl) ethanol:** Purified by chromatography on silica gel (1:1 pentane: ethyl ether), clear liquid (61%); ^{1}H NMR ($CDCl_3$, 400MHz) δ: 1.85 (s, 1H), 2.3 (s, 3H), 2.8(tt, 1H), 3.85(d, 2H), 7.1 (d 2H), 7.22 (d, 2H).

d_1-2-(4-nitrophenyl) ethanol: Purified by chromatography on silica gel (1: 1 pentane: ethyl ether), clear liquid (50%); ^{1}H NMR ($CDCl_3$, 400MHz) δ: 1.85 (s, 1H), 2.95(tt, 1H), 3.85(d, 2H), 7.5(d, 2H), 8.2(d, 2H).

***d_1*-2-(4-trifluorophenyl) ethanol:** Purified by chromatography on silica gel (1: 1 pentane: ethyl ether), clear liquid (50%); ^{1}H NMR ($CDCl_3$, 400MHz) δ: 1.75 (s, 1H), 2.8(tt, 1H), 3.75(d, 2H), 7.3 (d, 2H), 7.4 (d, 2H).

c. General procedure for synthesizing S-methyl xanthates [66]

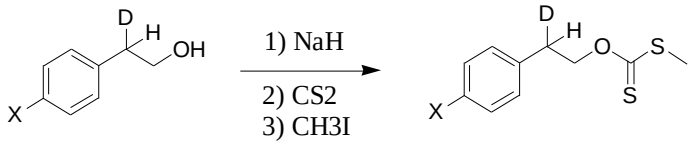

X = H, OCH_3, CH_3, Cl, NO_2, CF_3

Figure 24.The reaction scheme for the synthesis of S-methyl xanthates

Sodium hydride (60% w/w in mineral oil, 140mmol, 2.5 equiv.) was placed in a dry, nitrogen purged 2000ml 2-neck RBF. 600 ml anhydrous THF was added to the RBF, followed by the corresponding phenylethanol (56mmol). The reaction mixture was stirred at ambient temperature for 30 minutes and then carbon disulfide (4.2ml, 5.3g, 70mmol, 1.25 equiv.) was added, followed by another 30-minute stir. Iodomethane (4.4ml, 10.03g, 70mmol, 1.25 equiv.) was added. The reaction mixture was stirred for 30 minutes and then quenched with acetic acid solution (10ml glacial acetic acid in 500ml deionized water). The product was extracted with 3×200ml ethyl ether. The collected organic layers were washed with 500ml saturated sodium chloride solution and dried by magnesium sulfate. Ethyl ether was removed by rotary evaporation under reduced pressure. The product was purified by flash column chromatography under conditions provided bellow.

S-methyl O-(d_1-2-phenylethyl) xanthate (*d_1*-1): Purified by chromatography on silica gel (9:1 pentane: dichloromethane), light yellow oil (82%); ^{1}H NMR ($CDCl_3$, 400MHz) δ: 2.5(s, 3H), 3.05(tt, 1H), 4.78(d, 2H), 7.2-7.4 (m, 5H).

S-methyl O-(d_2-2-phenylethyl) xanthate (*d_2*-1): Purified by chromatography on silica gel (9:1 pentane: dichloromethane), light yellow oil (63%); ^{1}H NMR ($CDCl_3$, 400MHz) δ: 2.5(s, 3H), 4.76(s, 2H), 7.2-7.4 (m, 5H).

S-methyl O-(2-phenylethyl) xanthate (1): Purified by chromatography on silica gel (9:1 pentane: dichloromethane), light yellow oil (61%); ^{1}H NMR ($CDCl_3$, 400MHz) δ: 2.5(s, 3H), 3.05(t, 2H), 4.78(t, 2H), 7.2-7.4 (m, 5H).

S-methyl O-(d_1-2-(4-methoxyphenyl) ethyl) xanthate: Purified by chromatography on silica gel (9:1 pentane: ethyl ether), light yellow oil (63%); ^{1}H NMR ($CDCl_3$, 400MHz): δ 2.5(s, 3H), 3.05(tt, 1H), 4.78(d, 2H), 6.85 (d, 2H), 7.1 (d, 2H).

S-methyl O-(d_1-2-(4-methylphenyl) ethyl) xanthate: Purified by chromatography on silica gel (pentane), light yellow oil. ^{1}H NMR ($CDCl_3$, 400MHz) δ: 2.3 (s, 3H), 2.5(s, 3H), 3.05(tt, 1H), 4.78(d, 2H), 7.0-7.2 (m, 4H).

S-methyl O-(d_1-2-(4-chlorophenyl) ethyl) xanthate: Purified by chromatography on silica gel (pentane), light yellow oil. ^{1}H NMR ($CDCl_3$, 400MHz) δ: 2.3 (s, 3H), 2.5(s, 3H), 3.05(tt, 1H), 4.78(d, 2H), 7.1 (d 2H), 7.22 (d, 2H).

S-methyl O-(d_1-2-(4-nitrophenyl) ethyl) xanthate: Purified by chromatography on silica gel (pentane), yellow powder. ^{1}H NMR ($CDCl_3$, 400MHz) δ: δ2.5(s, 3H), 3.2(tt, 1H), 4.8(d, 2H), 7.4(d, 2H), 8.2(d, 2H).

S-methyl O-(d_1-2-(4-(trifluoromethyl)phenyl)ethyl) xanthate: Purified by chromatography on silica gel (pentane), light yellow oil. ^{1}H NMR ($CDCl_3$, 400MHz) δ: 2.45(s, 3H), 3.15(tt, 1H), 4.72(d, 2H), 7.3(d, 2H), 7.5(d, 2H).

2.5.2. Procedure for KIE Measurement

A 25 ml, 3-neck RBF was assembled with a condenser on the middle neck and an adapted thermocouple (*J-KEM type J*) on one of side necks. Octadecane (6ml, 4.67g, pre-warmed to liquid) was added to the RBF and heated to the desired temperature under the regulation of the thermo-controller (*J-KEM Model 210*). 200µl substrate (pure mono-deuterated xanthate or a mixture of protiated and deuterated xanthates) was quickly added into the RBF through the third neck. The reaction was brought to completion for intramolecular KIE measurement or to halfway-done for intermolecular KIE measurement (monitored by NMR, **Table 4**).

Table 4. *The time required for Chugaev elimination of differently substituted xanthates to reach 40% completion or to complete.*

	40% CONVERSION	**COMPLETION**					
Substituent	-H	-H	$-OCH_3$	$-NO_2$	$-CH_3$	-Cl	$-CF_3$
290°C	-	5 min	5 min	5 min	-	-	-
270°C	2 min 20 sec	25 min	15 min	20 min	20 min	20 min	20 min
250°C	5 min	2.5 h	30 min	3 h	-	-	-
230°C	40 min	5 h	3 h	5 h	-	-	-
210°C	3 h 20 min	30 h	-	-	-	-	-
200°C	4 h	40 h	8 h	20 h	-	-	-
190°C	15.5 h	68 h	70 h	68h	-	-	-
180°C	3 days	15 days	-	-	-	-	-

Note: (1) Intermolecular KIEs (HH/HD and HH/DD) were not measured at 290 °C because the reaction went too fast to be brought halfway-done in a reliable way. (2) 50 mg 1,3,5-trimethoxybenzene was added as an internal standard in experiments at 180°C and 190°C to insure the accuracy of the fractional conversion measurement. This pre-caution was taken to avoid the influence caused by the evaporation of styrene over long experimental duration.

The reaction mixture was then cooled down to around 40℃ in a cold water bath. The thermocouple and the condenser were rinsed down with 3 ml pentane so that all the products could be collected. The products (for intramolecular KIE measurement) or the remaining reactants (for intermolecular KIE measurement) were isolated and purified by column chromatography with pentane, and then analyzed by Varian 400MHz NMR spectrometer. About 100 μl sample was dissolved in 0.5 ml $CDCl_3$ in 5 mm NORELL® 507-HP-7 NMR tube. The parameters used for the quantitative ^{1}H NMR measurement are in **Table *5***.

Table 5. *The parameters used for quantitative ^{1}H NMR measurement on Varian 400 MR spectrometer for the Chugaev elimination products and reactans.*

	Substituent	longest T_1[a] (s)	d_1[b] (s)	pw[c] (μs)	at[d] (s)	nt[e]	ss[f]	VT (°C)
Styrene	H	6.353	35	13	4	16	2	30
	OMe	5.065	26	14				
	NO_2	5.730	30	12.5				
	CH_3	5.964	30	13.5				
	Cl	5.876	30	14				
Xanthate	H	4.577	25	13.5				
	OMe	3.959	20	14				
	NO_2	3.768	20	13.5				
	CH_3	4.149	20	13.5				
	Cl	3.995	25	13.5				

[a] T_1 measurement experiment was setup by the "dot1" function in Agilent VnmrJ (previously Varian) software. [b] $d_1 \approx 5 \times T_1$ [c] pw = pulse width [d] at = acquisition time [e] nt = number of scan [f] ss = number of dummy scan

Chapter 3. Mechanistic Study of the Cope Elimination

3.1. Mechanistic Background and Synthetic Utility of the Cope Elimination

Cope elimination is the pyrolytic decomposition of tertiary amine oxides discovered by Cope in 1949.[67] The well accepted mechanism of the reaction is that the oxygen atom on the tertiary nitrogen center attacks the β-hydrogen atom and a cyclic five-member transition state is formed and then decomposed to an alkene and N,N-dialkylhydroxylamine.[48,54,68] The reaction has been found to be stereoselective and forms cis-alkene as the only or major product.[54,69] In synthetic chemistry, Cope elimination has been extensively utilized to install olefins stereoselectively to tertiary amine sites under mild conditions. [69,70]

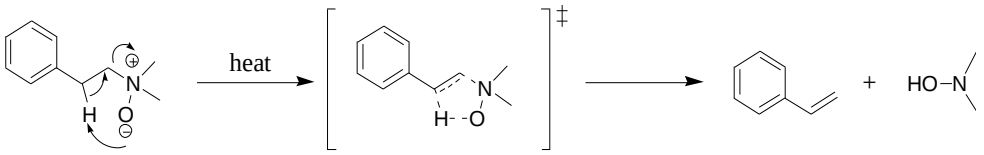

Figure 25. The well accepted mechanism of the Cope elimination reaction. The elimination of N,N-dimethyl-2-phenylethanamine oxide is illustrated as an example.

Cope elimination is different from other syn-β eliminations like ester pyrolysis and Chugaev elimination in several ways. First, Cope elimination has smaller reaction barrier and the reaction takes place with mild heating (85-115 °C).[48] The temperature for ester pyrolysis is 300-550 °C and Chugaev elimination is 100-250°C. Second, the transition state of ester pyrolysis and Chugaev elimination is a six-membered ring structure, while that of Cope elimination is a five-membered ring structure. Most importantly, the nucleophile -N-O^- in Cope elimination, is much more basic than -C=O and -C=S in ester thermolysis and Chugaev elimination, so Cope elimination is expected to be driven more by the abstraction of the β-hydrogen.

This chapter studies of the hydrogen transfer mechanism of the Cope elimination of 2-phenylethyldimethyl amine oxide and its para-substituted derivatives through kinetic isotope effect and linear free energy relationship (LFER). Whether Cope elimination deviates from the typical syn-β elimination mechanism will also be examined.

3.2. Methods

3.2.1. Intramolecular KIE measurement

Intramolecular competitive reaction (method (C) section 1.5) of the mono-deuterated 2-phenylethyldimethyl amine oxide (d_1-3-a ~ e) and its para-substituted derivatives were

performed to measure intramolecular KIE (Figure 26). Temperature dependence of the KIE was studied over the temperature range of 60°C-160°C for -OMe, -H and -CF_3 substituents.

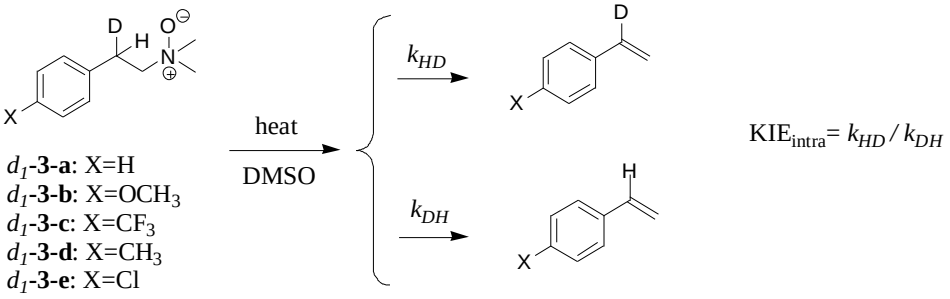

d_1-**3-a**: X=H
d_1-**3-b**: X=OCH_3
d_1-**3-c**: X=CF_3
d_1-**3-d**: X=CH_3
d_1-**3-e**: X=Cl

Figure 26. The scheme of intramolecular KIE measurement of the Cope elimination of 2-(p-substituted-phenylethyldimethyl amine N-oxide.

KIE experimental measurements carried out were summarized below:

Intramolecular KIE of d_1-**3-a** & d_1-**3-c** at: 60, 80, 100, 120, 140, 160°C.
Intramolecular KIE of d_1-**3-b** at: 60, 80, 100, 110, 120, 140, 160°C.
Intramolecular KIE of d_1-**3-d** & d_1-**3-e** at: 80°C.

3.2.2. LFER studies

Roughly equal amount of **3-a**, **b**, **c**, **d** and **e** (20 μl each) were mixed with 10 mg 1,3,5-trimethoxybenzene (internal standard) and dissolved in 0.5 ml DMSO-d_6. The resulting solution was placed in a NORELL® 509-UP-7 NMR tube and quantitative 13C NMR spectra were taken to determine the initial amount of each substrate relative to the internal standard. The mixture was heated to 80 °C or 120 °C, so the five substrate would undergo Cope elimination at the same time under the same condition. After 10 min at 80 °C or 1 minute at 120 °C, the reaction was quenched by chilling in ice-cold water.The solution in the NMR tube was measured again by ^{13}C NMR for the relative amount of each amine oxide remained after the reaction. Detailed procedure for taking quantitative ^{13}C NMR can be found in section 3.5.3. The rate constant for substituent X relative to that for subsituent H can be calculated from the relative fractional conversion F by Equation 36 based on the first-order rate law. The Hammett relationship (Equation 37) was then studied by analyzing the plot of $\ln(k_X/k_H)$ versus σ_{para}.

$$\frac{k_X}{k_H} = \frac{\ln(1-F_X)}{\ln(1-F_H)} \qquad \textit{Equation 36}$$

$$\ln(\frac{k_X}{k_H}) = \rho \cdot \sigma_X \qquad \textit{Equation 37}$$

3.3. Results and Discussion

3.3.1. The Temperature Dependence of the Intramolecular KIE for Three Different Substituents.

The temperature dependence of intramolecular KIE for Cope elimination is found to be influenced by the substituent at the para-position on the benzene ring 2-phenylethyldimethyl amine N-oxide (Figure 27). This is opposite to what is observed in Chugaev elimination.

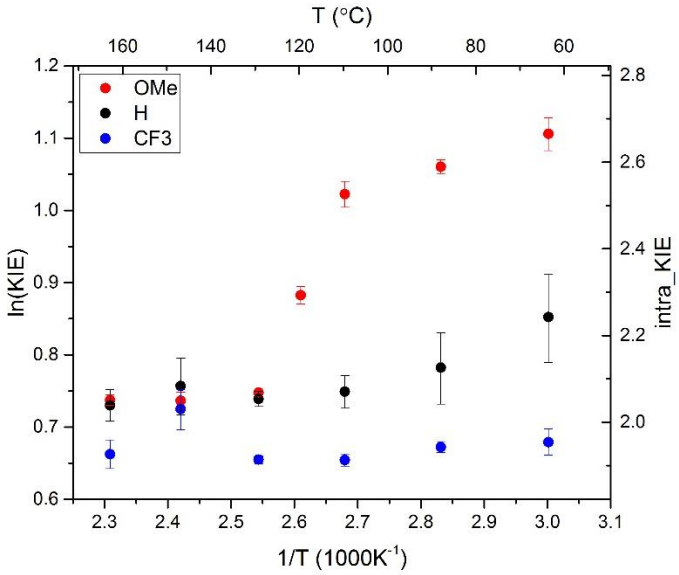

Figure 27. The Arrhenius plots of intramolecular KIE for H, methoxy (OMe) and trifluoromethyl (CF_3) substituted amine-oxides.

The reaction with the electronically neutral substituent -H has a small slope for the Arrhenius plot. The intramolecular KIE of reaction with the electron withdrawing group -CF_3 has temperature independent Arrhenius plot. The KIEs are consistently around 2.0 over 100 °C temperature range, meaning $E_{a,D}$-$E_{a,H}$ ≈0. More interestingly, the Arrhenius plot of the reaction with the electron donating group -OMe appears to be biphasic. There is a temperature independent phase in the high-temperature region (> 120 °C) and an increasing phase at the low-temperature region (< 110 °C).

The temperature independence in -CF_3 Arrhenius plot is unusual. Although ln(KIE) is expected to curve up and eventually plateau with decreasing temperatures (increasing 1/T) due to the presence of tunneling as discussed in section 1.4.2, the temperature independence region occurs at very low temperature (<100K, -173°C) and is unlikely to be reached at commonly accessible reaction temperatures.[13,71] Kwart et. al. studied the temperature dependence of the intramolecular KIE of Cope elimination of amine oxide with -H substituent (*d*$_1$-**3-a)** in diglyme and they also found a temperature independent Arrhenius plot (the KIE remained at ~2.2 between 91 °C to 210 °C).[55] The temperature independence was explained with a bent, cyclic transition structure.[56] (Our experiments

were carried out in DMSO solvent and were consistent with the results obtained by Kwart et. el. in the same solvent.[57])

Kwart's explanation with a bent TS is not satisfactory because it cannot explain the fact that the temperature dependence of the intramolecular KIE changes as a function of substituents. If a bent and cyclic TS is a common feature for Cope elimination, reactions with different substituents should exhibit similar temperature dependence. The dramatic change in the pattern of temperature dependence (biphasic temperature dependence for -OMe to temperature independence for -CF_3) leads to the guess that the nature of the structure of the TS changes as substituent changes. The TS structure change can be caused by change of reaction mechanism or change of rate-determining step.

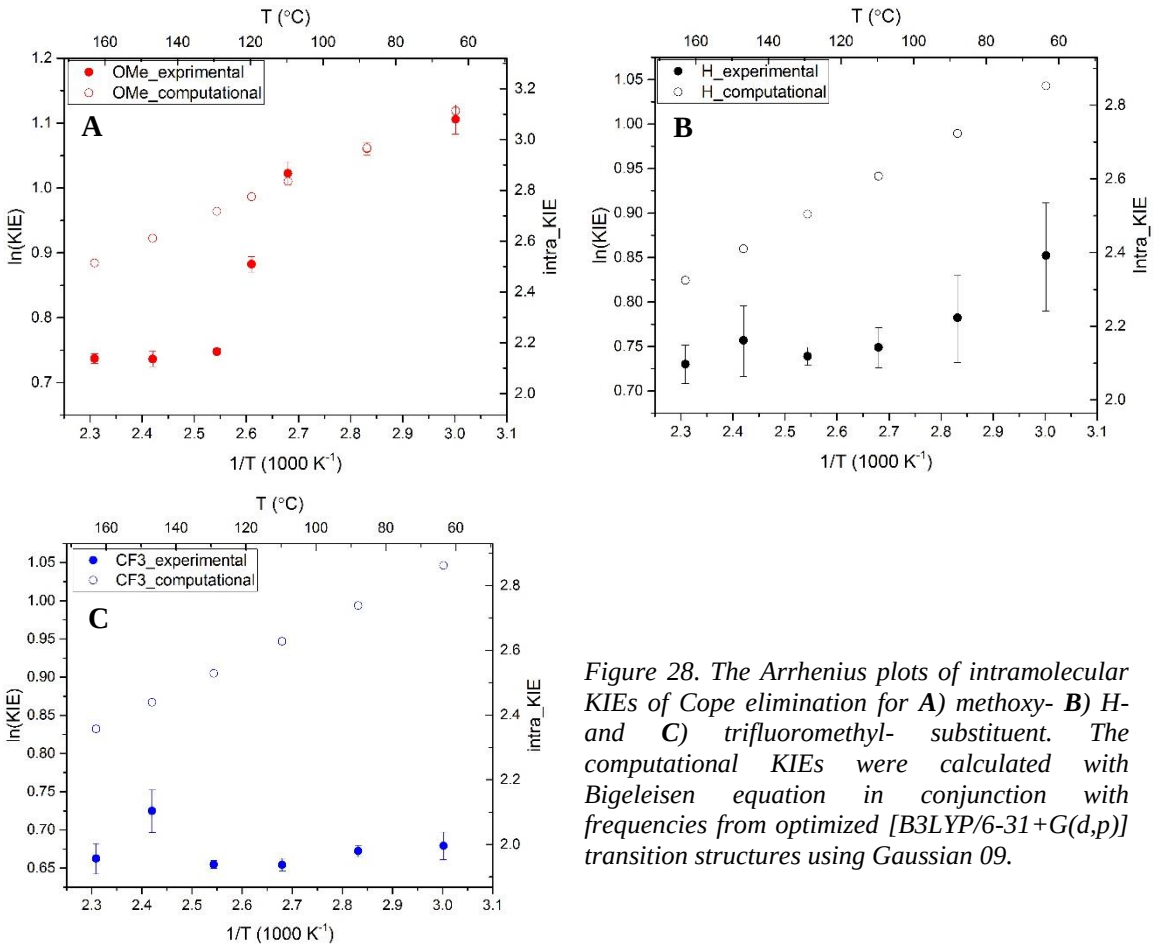

*Figure 28. The Arrhenius plots of intramolecular KIEs of Cope elimination for **A)** methoxy- **B)** H- and **C)** trifluoromethyl- substituent. The computational KIEs were calculated with Bigeleisen equation in conjunction with frequencies from optimized [B3LYP/6-31+G(d,p)] transition structures using Gaussian 09.*

Semiclassical KIEs were calculated with frequencies of the syn-β-elimination TS. The computational results were compared with the experimental ones (Figure 28). The slightly temperature dependent and temperature independent intramolecular KIEs for -H and -CF_3 are shown to be smaller than the semiclassical values in Figure 28 B, C. Most interestingly, the plots for -OMe show that the biphasic Arrhenius plot matches the semiclassical KIEs

at lower temperatures but is lower in value at higher temperatures (Figure 28A). The observations imply that 1) the Cope elimination for -OMe follows the syn-β-elimination mechanism and can be modeled by the syn-β-elimination transition state at high temperatures (120°C to 160°C); 2) Cope elimination reactions for -OMe at low temperatures (<110°C), -H and -CF_3, may go through another mechanism that generate smaller and temperature independent KIEs.

3.3.2. The LFER of the Cope Elimination.

The linear free energy relationship (LFER) was examined for the Cope elimination in order to understand the substituent effect on the temperature dependence. The reaction rates of Cope elimination were found to vary a lot with substituent species: ranging from 15 minutes for -CF_3 at to 18 hours for -OMe at 60 °C (**Table *6***). On the contrary, Chugaev eliminations with different substituent proceed in the same time scale (**Table *4***). The Hammett relationship was plotted with five various substituents (-OMe, -Me, -H, -Cl, -CF_3) at 80 °C and 120 °C (Figure 29). The Hammett plots at both temperatures have quasi-linear correlation ($R_2 \approx 0.92$). In both cases, the sensitivity constant Rho are larger than one ($\rho > 1$), meaning 1) the Cope elimination is sensitive to substituent more than the reference reaction (deprotonation of benzoic acid), and 2) significant amount of negative charge is built at the TS of the reaction.

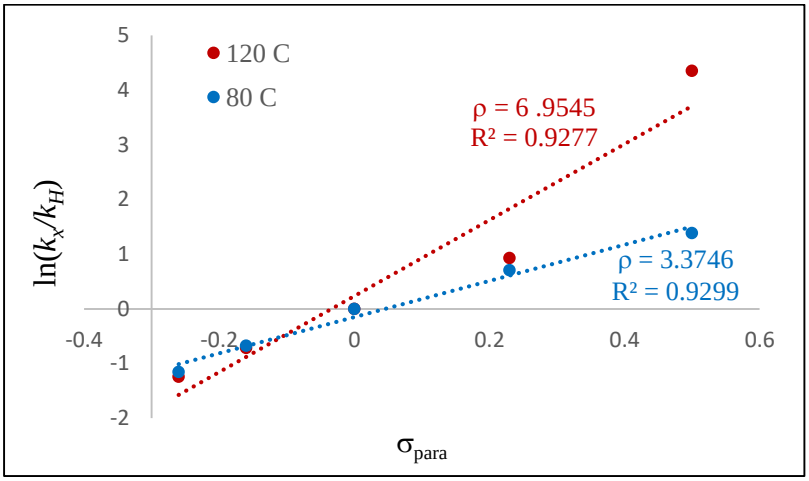

Figure 29. The Hammett plots ($ln(k_X/k_H)$ vs. σ_{para}) of the Cope elimination reaction at 80 °C and 120 °C.

Moreover, the Rho value at 120 °C is twice as much as the Rho value at 80 °C, which contradicts to what is expected by the Hammett equation (Equation 37). If the Cope elimination follows the same mechanism at different temperatures, the slope of the Hammett plot should decrease with increasing temperature ($\rho \propto \frac{\Delta G_H - \Delta G_X}{RT}$). The increased ρ at high temperatures indicate that Cope elimination shift to a mechanism that generate more negative charge at the transition state when more thermal energy is available. This second type of mechanism involved is very likely to be E1cB-elimination (unimolecular conjugate base elimination) mechanism, as the negatively charged oxygen in the amine

oxide is weakly basic (the pK_a of the conjugate acid is around 4.1) and the benzylic hydrogens are slightly acidic. At high temperature, -N-O^- abstracts a benzylic hydrogen and to generate a carbonanion that can be stabilized by the p-CF_3-benzene ring. In the following step, the double bond is formed and the leaving group (R_2NOH) is expelled.

3.4. Conclusion

The observations from the temperature dependence of experimental and computational intramolecular KIEs and LFER studies altogether point to the conclusion that Cope elimination has two competitive reaction mechanism: syn-β-elimination and E1cB-elimination. The former is a single-step process and the latter is a two-step process. The choice between the two types of mechanism is influenced by the substrate structure and the temperature.

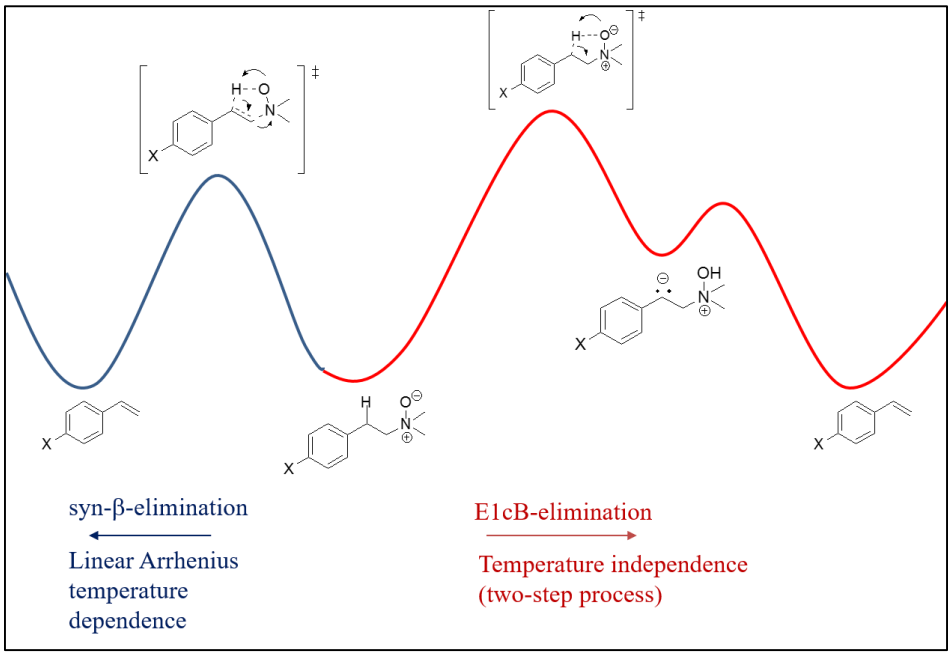

Figure 30. The potential energy diagram of the two types of possible reaction mechanism for Cope elimination.

The Cope elimination tend to undergo step-wise E1cB mechanistic pathway when there is an electron withdrawing group (e.g. -CF_3) on the benzene ring to stabilize the negative charge built at the TS, or excessive thermal energy to facilitate the hydrogen abstraction process. The intramolecular KIE measured in E1cB case is an averaged value resulted from a two-step reaction. With presence of electron donating group (e.g. -OMe), syn-β-elimination will dominate especially at low temperatures. In most of the cases, Cope elimination proceed through a mixture of the two types of mechanism. The temperature

effect on the two pathways can cancel each other out, resulting in temperature independence. The tunneling effect, which is expected to be a non-negligible component in the hydrogen transfer process in the Cope elimination, cannot be evaluated directly from the intramolecular KIE results due to the kinetic complexity.

3.5. Experimental Section

Chemicals: styrene (Sigma-Aldrich), 4-(trifluoromethyl)styrene (Sigma-Aldrich), 4-chlorostyrene (Sigma-Aldrich), 4-methylstyrene (Sigma-Aldrich), 4-methoxystyrene (Sigma-Aldrich), sodium borohydride (Sigma-Aldrich), sodium borodeuteride (Sigma-Aldrich), iodine (Sigma-Aldrich), 30% hydrogen peroxide solution (Fischer), 50 wt. % hydrogen peroxide solution (Sigma-Aldrich), sodium hydroxide (Sigma-Aldrich), triphenylphosphine (Sigma-Aldrich), bromine (reagent grade, Sigma-Aldrich), dimethylamine solution(2M in THF, Sigma-Aldrich), formaldehyde solution (37 wt. % in H_2O, Sigma-Aldrich), 88% formic acid (Fisher), tetrahydrofuran (THF) (anhydrous, Acros Organics), dimethyl sulfoxide (DMSO) (anhydrous, Acros Organics), magnesium sulfate(Fischer), pentane (Fischer), diethyl ether (Fischer), chloroform-d (Sigma-Aldrich), Acetone-d_6 (Sigma-Aldrich), 4Å Molecular Sieves (Fischer), Silica Gel (40-63μm, SORBTECH), deionized water (from household deionizer)

General: All reagents were commercially obtained otherwise noted. THF, DMSO and dichloromethane were dried by activated 4Å Molecular Sieves no longer than one week prior to use. 4Å Molecular Sieves were activated by flame-drying under vacuum. All reactions were carried out in flame-dried glassware and under N_2 atmosphere otherwise stated. Column chromatography was performed with silica gel (porosity 60Å, particle size 40-63μm) under reported solvent condition. Thin layer chromatography (TLC) were performed with Silica G TLC Plates from SORBENT TECHNOLOGIES. Developed TLC was viewed under an ultraviolet lamp. In temperature controlled reaction experiments, the temperature was regulated by J-KEM, Model 210 thermo-controller (with thermocouple type J). ^{1}H spectra were obtained on Varian 400 MR NMR spectrometer (400 MHz). The NMR data are reported as follows: chemical shifts (δ) in ppm, multiplicity (s=singlet, d=doublet, t=triplet, dd=doublet of doublets, tt=triplet of triplets, m=multiplet, br=broad), integration.

3.5.1. Material preparation

a. General procedure for synthesizing (2-bromoethyl) benzenes

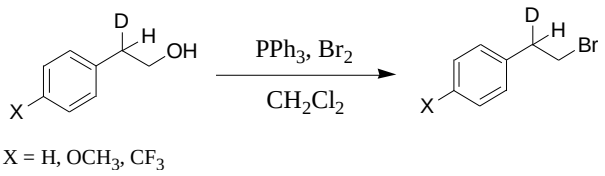

Figure 31. The reaction scheme for the synthesis of (2-bromoethyl) benzenes.

The d_1-para-substituted (2-bromoethyl) benzenes were synthesized by brominating the corresponding d_1-2-phenylethanol (Figure 31). The d_1-2-phenylethanols were synthesized from the corresponding styrene in the same way described in Chapter 2 section 2.5.1. To a dry 250 ml 2-neck round bottom flask, 100 ml anhydrous dichloromethane was added, followed by triphenylphosphine (5.13 g, 19.6 mmol, 1.2 equiv.). While stirring, bromine (1ml, 19.6 mmol, 1.2 equiv.) was added dropwise with caution. The solution turned murky and white after the addition of bromine. The solution was stirred for 30 minutes. The corresoponding d_1-2-phenylethanol (16.3 mmol) was added to the solution and the reaction mixture turned clear soon. The reaction mixture was stirred for one hour. 300 ml pentane was added to decrease the solubility of the by-product triphenylphosphine oxide ($O=PPh_3$). The solution was stirred for 3 hours and then filtered to get rid of the white precipitate $O=PPh_3$. The filtrate was condensed to 50 ml by rotary evaporator under reduced pressure. Repeat the pentane addition (100 ml) and filtration procedure until no white precipitate was formed. The solvent was removed by rotary evaporation and the product was obtained. The physical appearance and ^1H NMR peaks of each product are listed below:

***d_1*-1-(2-bromoethyl) benzene:** clear liquid; ^1H NMR ($CDCl_3$, 400MHz) δ: 3.05(tt, 1H), 3.43(d, 2H), 7.08-7.23 (m, 5H).

***d_1*-1-(2-bromoethyl)-4-methoxy benzene:** clear liquid; ^1H NMR ($CDCl_3$, 400MHz) δ: 2.94(tt, 1H), 3.36-3.38(d, 2H), 3.64(s, 3H), 6.7(d,2H), 6.99(d, 2H).

***d_1*-1-(2-bromoethyl)-4-(trifluoromethyl) benzene:** clear liquid; ^1H NMR ($CDCl_3$, 400MHz) δ: 3.2(tt, 1H), 3.55(d, 2H), 7.33(d,2H), 7.56(d, 2H).

b. General procedure for synthesizing (para-substituted) phenylethyl dimethylamines

(i) From bromoethyl benzenes via S_N2 reaction:

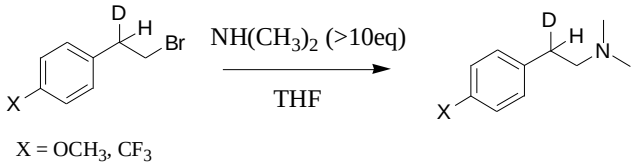

Figure 32. The synthesis of (para-substituted) phenylethyl dimethylamines from bromoethylbenzenes.

In a dry 150 ml 2-neck RBF that was equipped with a stir bar and assembled with a 50 ml additional funnel at the upright neck, add 50ml 2M dimethylamine (80 mmol, 12.5 equiv.) THF solution through the side neck. The corresponding (2-bromoethyl) benzene (6.1 mmol) was dissolved in 15 ml anhydrous THF, and the resulting solution was transferred into the additional funnel. While stirring the solution in the RBF, the (2-bromoethyl) benzene THF solution was added slowly drop-by-drop to the RBF by adjusting the stopper of the additional funnel. This process took up to several hours. After the completion of the addition, the solution is stirred for 3 hours. The solution was filtered through a piece of cotton and then condensed by rotary evaporation. The resulting colorless liquid is the phenylethyl dimethylamine.

***d*$_1$-N,N-Dimethylphenethylamine:** colorless liquid; ^{1}H NMR ($CDCl_3$, 400MHz) δ: 2.29(s, 6H), 2.51-2.53(d, 2H), 2.73-2.77(tt, 1H), 7.16(d, 2H), 7.23(d, 2H).

***d*$_1$-N,N-Dimethyl-4-methoxyphenethylamine:** colorless liquid; ^{1}H NMR ($CDCl_3$, 400MHz) δ: 2.26(s, 6H), 2.45(d, 2H), 2.68(tt, 1H), 3.75(s, 3H), 6.78(d, 2H), 7.08(d, 2H).

***d*$_1$-N,N-Dimethyl-4-(trifluoromethyl)phenethylamine:** colorless liquid; ^{1}H NMR ($CDCl_3$, 400MHz) δ: 2.28(s, 6H), 2.52(d, 2H), 2.79(tt, 1H), 7.27(m, 2H), 7.51(m, 2H).

(ii) From the phenylethylamine through Eschweiler-Clarke reaction:

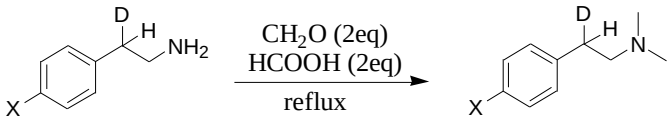

X = CH_3, Cl

Figure 33. The synthesis of (para-substituted) phenylethyl dimethylamines from phenylethylamine.

d$_1$-2-(4-methyl-phenylethyl)amine and *d*$_1$-2-(4-chloro-phenylethyl)amine was obtained from another graduate student Thomas Giagou in our lab and was synthesized from the corresponding benzaldehyde through another pathway. In a dry 2-neck 25ml RBF that is equipped with a condenser, 7.5ml deionized water was added, followed by the corresponding phenylethylamine (3.12 mmol) and 37% formaldehyde solution (6.24 mmol). The solution was stirred for 5 minutes. 88% formaldehyde solution (6.24 mmol) was added. The reaction mixture was stirred and refluxed for 3 days. After cooling down, sodium hydroxide (3.12 mmol) was added. The solution was stirred for 10 minutes, and then extracted with 3×3ml ethyl ether. The solvent was removed by rotary evaporation.

***d*$_1$-N,N-Dimethyl-4-methylphenethylamine:** colorless liquid; ^{1}H NMR ($CDCl_3$, 400MHz) δ: 2.26(s, 6H), 2.28(s, 3H), 2.46-2.50(d, 2H), 2.7(tt, 1H), 7.06 (s, 4H).

***d*$_1$-N,N-Dimethyl-4-chlorophenethylamine:** colorless liquid; ^{1}H NMR ($CDCl_3$, 400MHz) δ: 2.25(s, 6H), 2.45-2.49(d, 2H), 2.7(tt, 1H), 7.1(d, 2H), 7.2(d, 2H).

c. General procedure for synthesizing N,N-dimethyl-2-phenylethanamine oxides

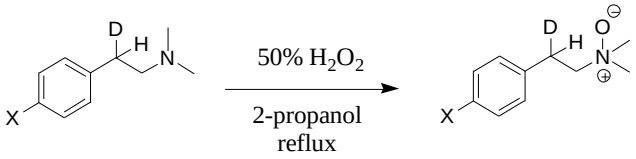

X = H, OCH_3, CF_3, CH_3, Cl

Figure 34. The synthesis of (para-substituted)phenylethyl dimethyl amine oxides.

In a 50ml 2-neck RBF with one neck connected to a condenser, add 10 ml 2-propanol, followed by the corresponding (para-substituted) phenylethyldimethylamine (4.58 mmol) and 2ml hydrogen peroxide. The reaction mixture was stirred at heated at 60 °C for 24 hours. After the reaction completed, the solvents (2-propanol and water) were removed by a belt vacuum pump with an acetone/dry ice cold trap. The structure of the products was confirmed by ^{1}H NMR with Acetone-d_6 or D_2O as the solvent for better solubility of the product and peak separation than $CDCl_3$.

N,N-dimethyl-2-phenylethanamine oxide: viscous colorless liquid; ^{1}H NMR (Acetone-d_6, 400MHz) δ: 3.25 (t, 1H), 3.33 (s, 6H), 3.59-3.61 (d,2H), 7.22-7.36 (m, 5H).

N,N-dimethyl-2-(4-methoxyphenyl)ethylamine oxide: viscous colorless liquid; ^{1}H NMR (Acetone-d_6, 400MHz) δ: 3.15 (t, 1H), 3.34 (s, 6H), 3.57-3.59 (d,2H), 3.73 (s, 3H), 6.83-6.85 (d, 2H), 7.24-7.26 (d, 2H).

N,N-dimethyl-2-(4-(trifluoromethyl)phenyl)ethylamine oxide: viscous colorless liquid; ^{1}H NMR (D_2O, 400MHz) δ: 3.15 (t, 1H), 3.28 (s, 6H), 3.58 (d,2H), 7.33-7.36 (d, 2H), 7.39-7.41 (d, 2H).

N,N-dimethyl-2-(4-methylphenyl)ethylamine oxide: viscous colorless liquid; ^{1}H NMR (Acetone-d_6, 400MHz) δ: 2.26(s, 3H), 3.18 (t, 1H), 3.35 (s, 6H), 3.60 (d,2H), 7.1 (d, 2H), 7.2 (d, 2H).

N,N-dimethyl-2-(4-chlorophenyl)ethylamine oxide: viscous colorless liquid; ^{1}H NMR (Acetone-d_6, 400MHz) δ: 3.25 (t, 1H), 3.34 (s, 6H), 3.63 (d,2H), 7.28-7.30 (d, 2H), 7.35-7.37 (d, 2H).

3.5.2. The Procedure for KIE measurements

A 25 ml, 3-neck RBF was fitted with a condenser in the middle neck and a thermocouple (*J-KEM type J*) in one of the side necks. 9.5 ml DMSO was added to the RBF and heated to the desired temperature under the regulation of the thermo-controller (*J-KEM Model 210*). 150 µl amine oxide was dissolved in 0.5 ml DMSO and the resulting solution was quickly added through the third neck into the round bottom flask. The reaction was brought

to completion for intramolecular KIE measurement (the time needed for differently substituted amine oxides at each experimental temperature is shown in **Table 6**). After the reaction completed, the mixture was then cooled down in a cold-water bath. The thermocouple and the condenser were rinsed down with 3 ml pentane so that all the products could be collected. The mixture was transferred to a reparatory funnel and extracted by 2 ml pentane for four times. The combined organic layers were condensed by rotary evaporation under reduced pressure. The isolated products (styrene) were then analyzed by quantitative ^{1}H NMR (the same conditions and parameters used for the corresponding styrene in the Chugaev elimination study **Table *5*** were applied).

Table 6. *The reaction time for each substituted amine oxide at various experimental temperatures.*

	-H [a]	-OCH_3	-CH_3	-Cl	-CF_3
160 °C	3 min	4 min [b]	--	--	< 3 min
140 °C	15 min	15 min [b]	--	--	< 3min
120 °C	40 min	40 min [b]	--	--	5 min
110 °C	--	55 min	--	--	--
100 °C	2 h 40 min	2 h 45min	--	--	5 min
80 °C	5 h	5 h	15 min	40 min	10 min
60 °C	18 h	18 h	--	--	15 min

[a] Experiments performed by Thomas Giagou (previous PhD student); [b] Experiments partly (1 to 3 replica out of 5) performed by Thomas Giagou.

3.5.3. T_1 Measurement for ^{13}C NMR in the LFER study

In order to measure the amount of each substituted amine oxide relative to the internal standard precisely, the recycle delay d_1 parameter needs to be calibrated in order to generate ^{13}C NMR spectra whose peak intensity is proportional to the concentration of the corresponding chemical species (quantitative NMR). d_1 is determined by the spin-lattice relaxation time (T_1). The recycle delay d_1 should be about five times T_1 in quantitative NMR measurement.

T_1 is measured by the "inversion-recovery" [72,73] method in the following steps (the sample for NMR measurement was prepared as described in section 3.2.2.):

First, a 180°- τ -90° pulse sequence for ^{1}H decoupled ^{13}C measurement experiment was brought up and copied to a new directory. d_1 was set to be an estimated sufficient value for most ^{13}C signals (usually 60 ~100 sec, and d_1=100 sec was used for this work). The delay time τ (d_2 in this NMR experiment on the TopSpin software for Bruker NMR) between the two pulses was set to be zero. The resulting spectrum was phased so that all the peaks are inverted. The phased spectrum was saved.

Second, eleven experiments of 180°- τ -90° pulse sequence were set up with d_1 = 60 sec, and d_2 = 4, 5, 6, 7, 8, 9, 10, 11, 12, 13, 14 sec respectively. The resulting spectra were

phased applying the same phasing parameters (PHCO, PHC1) used for the spectrum obtained in the first step (d_1 = 60 sec, d_2 = 0 sec).

Finally, the twelve spectra from the previous two steps were compared, and the one with vanished peaks or peaks starting to turn up was identified and the d_2 was recorded. T_1 was then calculated by Equation 38.

$$T_1 = \frac{d_{2,null}}{\ln 2} \qquad \textit{Equation 38}$$

In the experiment for the Cope elimination LFER study, peaks were found to flip at $d_{2,null}$=12 sec, so T_1 was calculated to be 17 sec and $d_1 = 5 \times T_1$ = 85 sec.

Chapter 4. Mechanistic Study of Ru-Catalyzed C-H functionalization

4.1. Synthetic Utility and Mechanistic Background of the Du Bois C–H Amination

C-H amination in which a nitrenoid (a metal complex coordinated nitrene) inserts into a ubiquitous carbon-hydrogen bond is a new C-H functionalization method developed within the last two decades and has broad potential to become enabling technology for drug discovery and synthesis.[72] C-H functionalization has been an active area of research and has drawn much attention to the chemistry community due to its advantages over classical organic synthesis: (1) The method can access wider range of modification sites on organic molecules compared to the traditional functional group modification method that is restricted to the locations of reactive functional groups; (2) The method can avoid complex multi-step synthesis and enables the economical synthesis of potential pharmaceutical target compounds.[72,73] Earlier approaches to functionalize C-H bonds are through the insertion of reactive metal complex into a C-H bond by oxidative addition or metathesis etc. and are generally called "C-H activation".[74,75] Functionalizing C-H bonds by reactive metal-carbene or metal-nitrene offers an alternative approach and is more economic (high turnover number) and more selective.[72,76-78]

Given the ubiquity of nitrogen atoms in biologically active compounds, C-H amination is a valuable synthetic method and is likely to find widespread application in pharmaceutical industry. The intramolecular C-H amination method developed by Du Bois and colleagues has already demonstrated success in synthesizing complex natural products in stereoseletive fashion.[79-81] However, compared to its analogous reactions of metal carbenes, the reactions of metal nitrenes are still less developed.[72,82] The mechanism of nitrenoid mediated C-H functionalization has not been well established yet, which is one major factor

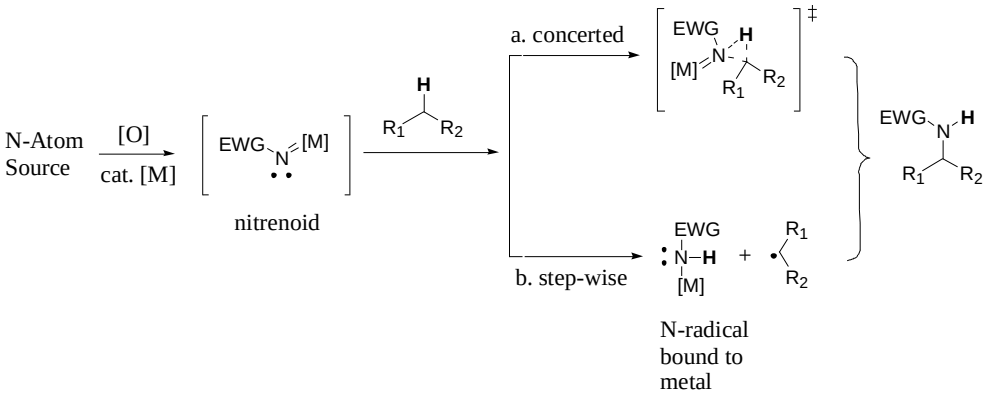

Figure 35. Possible mechanisms for C-H amination with metal-nitrene.[18,83]

that impedes the development of C-H amination. Most publications on this topic focus on reporting the outcomes of scanning the catalyst design, substrate scope and reaction conditions, and only a few research projects include mechanistic studies[18,84,85].

There are two mechanistic questions need to be answered. The first question is whether the new carbon-nitrogen bond forms through a single-step direct nitrenoid insertaion or a stepwise procedure during which a hydrogen atom is abstracted and a diradical species is formed first and the C-N bond is formed in the following step (*Figure 35*). The second question is closely related to the first question and it interrogates the multiplicity of the nitrene. If the reactive nitrene is a triplet, the diradical pathway is more likely to happen; and if the nitrene is in singlet state, the concerted pathway dominates.

To address the knowledge gap in C-H amination mechanism, the new reaction using a sulfamate (**4**) as the nitrogen source, tetrakis(2-oxypyridinato)diruthenium(II, III) chlroride $[Ru_2(hp)_4]Cl$ as the catalyst, and bis(tert-butylcarbonyloxy)iodobenzene ($PhI(O_2C^tBu)_2$) as the oxidant was studied through kinetic isotope effect (Figure 36). This reaction was reported very recently by Du Bois and collegues and was found to favor C-H bond amination to π-bond functionalization to form cyclic structure (~7:3) when the substrate is unsaturated.[84] $[Ru_2(hp)_4]Cl]$ provides chemoselectivity that contradicts to its structural analogy $Rh_2(OAc)_4$ and is a promising catalyst. The experimental and computational studies reported suggest that $[Ru_2(hp)_4]Cl]$-catalyzed reaction go through a stepwise mechanism.[84] Temperature dependence of intra-molecular KIE, intermolecular KIE and computational studies were carried out in this research project to gain more insights into the reaction mechanism.

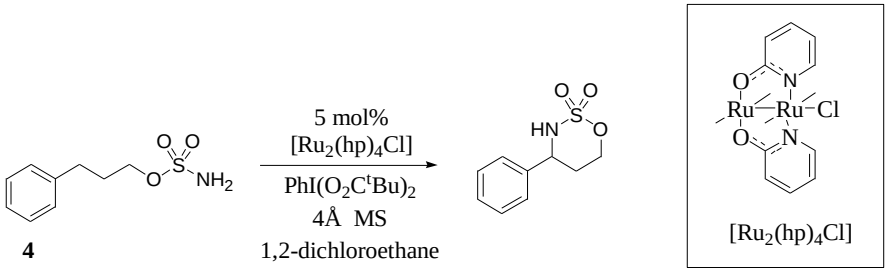

*Figure 36. $[Ru_2(hp)_4]Cl]$-catalyzed C-H amination of 3-phenylpropyl sulfamate (**4**).*

4.2.Method

4.2.1. Intramolecular KIE

Intramolecular KIE for ruthenium catalyzed C-H amination was measured by quantifying the deuterium fractionation in the products generated from 2,3-d_2-3-phenylpropyl sulfamate (d_2-**4**) (Figure 37). The measurement was carried out for three times at each of the temperatures: 0 °C, 20 °C, 40 °C, 60 °C, 80 °C.

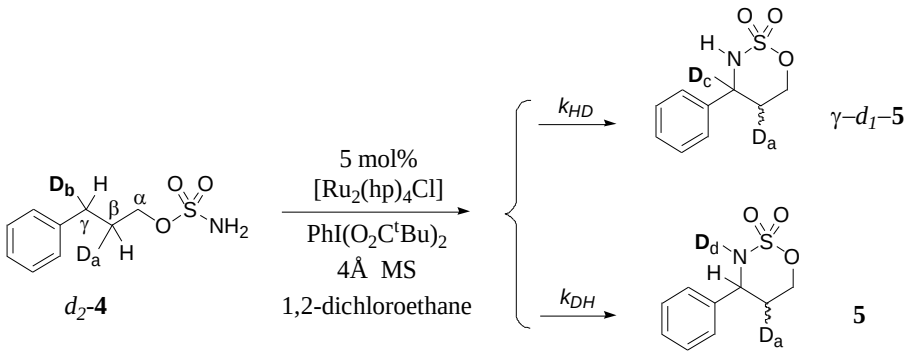

Figure 37. A scheme that demonstrates the intramolecular competition between C-H vs. C-D functionalization catalyzed by [Ru₂(hp)₄Cl].

Deuterium (^{2}H) NMR was used to quantify the product ratio as it gave cleaner spectra and thus more accurate KIE results. The deuterium label at the γ position (D_b) undergoes reaction (either being transferred to the nitrogen or staying on the same carbon but transformed from a secondary to a tertiary hydrogen) and is where the intramolecular KIE is produced. On the other hand, the deuterium label at the β position (D_a) keeps intact during the reaction and serves as an internal reference. β and γ position in *d₂*-**4** have equal deuterated rate (D_a=D_b), which was confirmed by ^{2}H NMR. The exchangeable amine hydrogen D_d was found to be lost after work-up and purification process (being exchanged with H_2O in the environment) and was not used for KIE calculations. According to *Equation 16*, the intramolecular KIE for C-H amination can be calculated via: $KIE_{intra} = \frac{[\gamma - d_1 - \mathbf{5}]}{[\mathbf{5}]} = \frac{[D_c]}{[D_a]-[D_c]}$.

4.2.2. Intermolecular KIE

Intermolecular competitive reactions were carried out between *β-d₁*-**4** and *d₂*-**4** as shown in Figure 38. The same as in the intramolecular KIE measurement, the deuterium label D_a serves as an internal reference label, and ^{2}H NMR is used to measure the isotopomers ratio. The initial and final ratio (R_o and R) between the reactants *β-d₁*-**4** and *d₂*-**4** were determined from the integration values of D_a, D_b, $D_{a'}$ and $D_{b'}$. The intermolecular KIE is calculated with *Equation 35* based on method (B) in section 1.5.

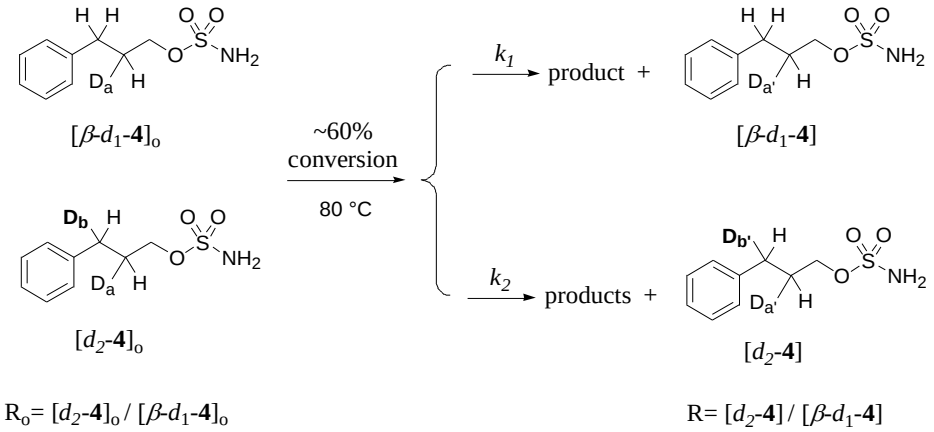

Figure 38. A scheme that illustrates the intermolecular KIE experimental design for Ru-catalyzed C-H amination.

4.3.Results and Discussion

4.3.1. Temperature Dependence of Intramolecular ^{2}H KIEs

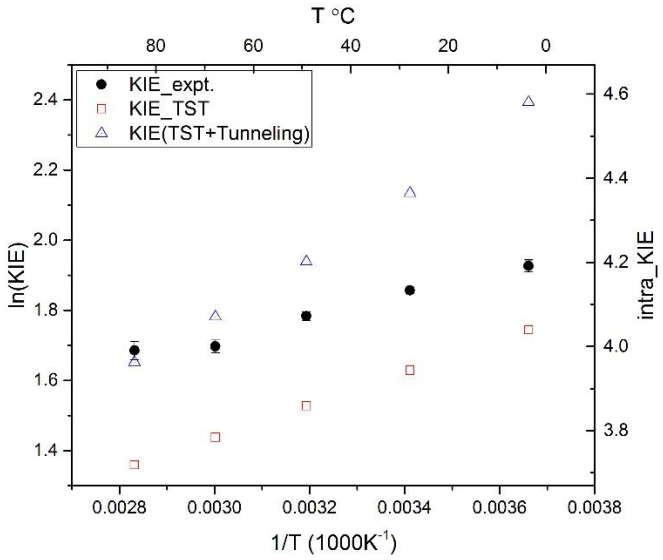

Figure 39. The Arrhenius plot of the intramolecular KIE of the Ru-catalyzed C-H amination.

The intramolecular KIEs of the [$Ru_2(hp)_4$]Cl] catalyzed C-H amination of d_2-**4** were observed to be from 6.86 to 5.39 over the temperature range of 0 °C to 80 ºC. These values are smaller than what is expected for the H-atom abstraction process (KIE ≈ 12-14). The observed values are probably diminished by the secondary KIE in the same manner as in the Chugaev elimination (see Chapter 2). The plot of ln(KIE) vs 1/T was found to be very linear (R^2=0.98). The Arrhenius pre-exponential factor ($\ln(A_H/A_D)$) is 2.78 (larger than 1.2, indicating tunneling).

The intermolecular KIE was measured for the reaction at 80 ºC and was close to 1 (0.98), indicating that the H-atom abstraction step is not the rate-determining step. The nitrenoid formation usually has the highest energy barrier and thus the rate-determining step in the metal-mediated C-H functionalization.[5] As a result, the intermolecular KIE is not useful for studying the H transfer process in this case. Computational study may provide some useful information (such as the primary and secondary KIE that cannot be measured by experiments) if appropriate model is available.

4.3.2. The Effect of Magnetic Field on the Intramolecular KIE of the Ru-catalyzed C-H Amination

In order to probe the multiplicity of the reactive metal-nitrene species, the effect of external magnetic field on intramolecular KIE was explored. The experimental design is based on the principle of energy quantization of particles with non-zero spin angular momentum (paramagnetic). A particle with gyromagnetic ratio γ and magnetic quantum number m will shift in energy by the amount of $E_{magnetic}$ in an external field of strength B.

$$E_{magnetic} = -\hbar\gamma Bm \qquad \textit{Equation 39}$$

It was proposed that the nitrene in Ru-catalyzed C-H amination reaction has a triplet ground state and when coordinate with the quartet $[Ru_2(hp)_4]Cl]$ catalyst becomes a doublet species.[84] The energy of the doublet nitrenoid complex is expected to change in a magnetic field and may be hopefully reflected in the value of the KIE (decreasing with increasing magnetic field).

The C-H amination of the sulfamate d_2-**4** catalyzed by $[Ru_2(hp)_4]Cl]$ was prepared in an NMR tube and let to proceed inside an NMR spectrometer to take advantage of the strong magnetic field generated consistently by the machine. Intramolecular KIE was measured for reaction in the magnetic field of the 400 MHz NMR and 600 MHz NMR, and compared with the results obtained in the magnetic field of earth.

Table 7. *Intramolecular KIE of Ru-catalyzed C-H amination in three different external magnetic fields.*

External Magnetic Field	~ 0 T	9.4 T [a]	14.1 T [b]
KIE_{intra}	5.9 ± 0.10	5.9 ± 0.04	5.8 ± 0.07

[a] generated by Varian 400 MHz NMR spectrometer [b] generated by Bruker 600 MHz NMR spectrometer

As ***Table 7*** shows, no significant difference was observed between the intramolecular KIEs taken in various external magnetic field. This negative results may due to the tininess and complexity of the magnetic field induced energy split. The energetic change of the nitrenoid in a magnetic field may be too trivial to be measured by KIE. In addition, the nitrene is such reaction is not in free state but bound to a metal (ruthenium in this case) that

has non-zero net spin angular momentum and produce a local magnetic field that makes the situation more complicated. Electron spin resonance (ESR) spectroscopy that measure the energy split of electrons instead of atomic nuclei may be useful to determine the electronic nature of metal-nitrenes and metal-carbenes.

4.3. Experimental Section

Chemicals: cynnamyl alcholol (98%, Sigma-Aldrich), lithium aluminum hydride (Sigma-Aldrich), lithium aluminum deuteride (Sigma-Aldrich), deuterium oxide (Sigma-Aldrich), tetrahydrofuran (THF) (anhydrous, Acros Organics), chlorosulfonyl isocyanate (98%, Sigma-Aldrich), formic acid (Sigma-Aldrich), acetonitrile (Sigma-Aldrich), dimethylacetamide (Fischer), ruthium (III) chloride hydrate (ReagentPlus, Sigma-Aldrich), acetic anhydride (Sigma-Aldrich), acetic acid (Sigma-Aldrich), lithium chloride (Sigma-Aldrich), 2-hydroxypyridine (97%, Sigma-Aldrich), chlorobenzene (Sigma-Aldrich), bis(tert-butylcarbonyloxy)iodobenzene (97%, Sigma-Aldrich), 1,2-dichloroethane (anhydrous, Sigma-Aldrich), magnesium sulfate(Fischer), sodium sulfate (Fisher), pentane (Fischer), ethyl ether (Fischer), chloroform-*d* (Sigma-Aldrich), benzene-d_6 (Sigma-Aldrich), 4Å Molecular Sieves (Fischer), Silica Gel (40-63μm, SORBTECH), deionized water (from household deionizer), TLC Plates (SORBENT TECHNOLOGIES)

General: All reagents were commercially obtained otherwise noted. THF and 1,2-dichloroethane were dried by activated 4Å molecular sieves no longer than one week prior to use. 4Å molecular sieves were activated by flame-drying under vacuum no longer than one week prior to use and stored in tightly sealed container. All reactions were carried out in flame-dried glassware and under N_2 atmosphere otherwise stated. Column chromatography was performed with silica gel (porosity 60Å, particle size 40-63μm) under reported solvent condition. Thin layer chromatography (TLC) were performed with Silica Gel. Proton NMR spectra were obtained on Varian 400 MR NMR spectrometer (400 MHz). Deuterium NMR spectra were obtained on Bruker 600 MHz NMR. The NMR data are reported as follows: chemical shifts (δ) in ppm, multiplicity (s=singlet, d=doublet, t=triplet, dd=doublet of doublets, tt=triplet of triplets, q=quintet, qt=quintet of triplet, m=multiplet, br=broad), integration.

4.3.1. Material Preparation

a. The synthesis of 3-phenyl-1-propanols[86]

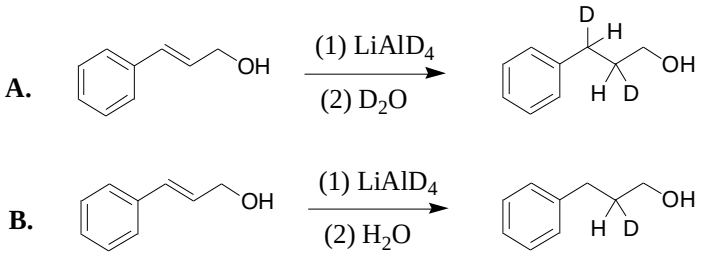

Figure 40. The synthesis of 3-phenyl-1-propanols. ***A.*** *2,3-d_2-3-pheyl-1-propanol;* ***B.*** *2-d_1-3-pheyl-1-propanol;*

In a 250 ml 2-neck RBF with a stir bar, add 50 ml anhydrous THF. Cynnamyl alcohol (5g, 37 mmol) was added to the RBF, the solution was stirred to allow the cynnamyl alcohol to dissolve. The solution was cooled down to 0 °C in an ice bath, after which lithium aluminum deuteride (1.56g, 37 mmol, 1 equiv.) was added. The solution was stirred overnight, and the ice bath was allowed to warm up to room temperature. Deuterium oxide (1ml, 56 mmol, 1.5 equiv., for 2,3-d_2-3-phenyl-1-propanol) or deionized water (1 ml ,56 mmol, 1.5 equiv., for 2-d_1-3-pheynl-1-propanol) or was added slowly and stirred for one hour (*Figure 40*). 200ml deionized water was added, and the mixture was extracted with 3×50ml ethyl ether. The combined organic layers were washed with saturated sodium chloride solution and then dried with magnesium sulfate. The solvent was removed by rotary evaporator under reduced pressure. The product was purified by chromatography on silica gel (55:45 pentane: ethyl ether).

2-d_1-3-phenyl-1-propanol: colorless liquid (65%); ^{1}H NMR ($CDCl_3$, 400MHz) δ: 1.46 (s, -OH), 1.88 (qt, H), 2.71 (d, 2H), 3.67 (d,2H), 7.19-7.21 (m, 3H), 7.26-7.31 (m, 2H).

2,3-d_2-3-pheyl-1-propanol: colorless liquid (80%); ^{1}H NMR ($CDCl_3$, 400MHz) δ: 1.35 (s, -OH), 1.87 (br m, H), 2.68 (d, H), 3.67 (d,2H), 7.19-7.21 (m, 3H), 7.26-7.31 (m, 2H).

b. The synthesis of the 3-phenylpropyl sulfamates[84,87]

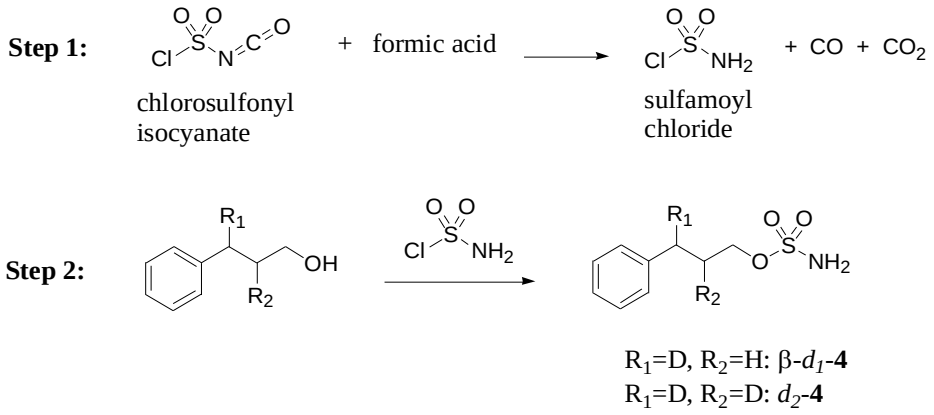

Figure 41. The general steps for synthesizyng 3-phenylpropyl sulfamates.

Formic acid (4 ml, 108 mmol, 3 equiv.) was added dropwise to ice cold chlorosulfonyl isocyanate (9.4 ml, 108 mmol, 3 equiv.) with vigorous stirring, in a 250 ml 2-neck round bottom flask. The mixture started to produce gases immediately and solidified within a few minutes. 37.5 ml acetonitrile was added to the white mass and the resulting clear solution was slowly warmed to room temperature over 5 hours. The flask was placed in an ice bath again. 3-phenylproplyl sulfamate (36 mmol) was dissolved in 15 ml dimethylacetamide and the resulting solution was added slowly in the ice cold reaction mixture in the round bottom flask. The reaction mixture was warmed up to room temperature and stirred overnight. 50 ml deionized water was added to quench the reaction. The mixture was extracted with 3×15ml ethyl ether. The combined organic layers were washed with brine and dried with sodium sulfate. The solvent was removed through rotary evaporation. The product was purified by chromatography on silica gel (2:3 pentane: ethyl ether).

2-*d*$_1$-3-phenylpropyl sulfamate (β-*d*$_1$-**4**): white solid (62%); ^{1}H NMR (C_6H_6, 400MHz) δ: 1.72 (t, 1H), 2.48-2.51 (d, 2H), 4.08 (d, 2H), 6.94-7.13 (m, 5H).

2, 3-*d*$_2$-3-phenylpropyl sulfamate (*d*$_2$-**4**): white solid (51%); ^{1}H NMR (C_6D_6, 400MHz) δ: 1.56 (m, 1H), 2.34-2.36 (d, 1H), 3.34 (s, -NH_2), 3.71 (d, 2H), 6.94-7.13 (m, 5H).

c. The preparation of [$Ru_2(OAc)_4Cl$]

Ruthenium (III) chloride hydrate (1g, 3.75 mmol) was combined with 25 ml glacial acetic acid, 7 ml acetic anhydride and lithium chloride (1g, 23.75 mmol, 6 equiv) in a 2-neck round bottom flask that was equipped with a condenser. The brown-black solution was heated under reflux while stirring for 3 days. Following this time, the solution was cooled to room temperature and the supernant was decanted. The solids were suspended in 20 ml ethyl ether and allow to settle to the bottom. The supernant was decanted. The remaining solids were transferred onto a Buchner funnel and washed with 10 ml deionized water, 10 ml acetone, and 10 ml ethyl ether. More ethyl ether was used to rinse the dark red solid until the filtrate becomes clear. The resulting solid was dried in a vacuum oven (80°C) to give clay-red powder (0.73g, 30%).

d. The preparation of [$Ru_2(hp)_4Cl$]

60 ml chlorobenzene was added in a 150 ml 2-neck round bottom flask, followed by 2-hydroxypyridine (0.57g, 6 mmol, 10 equiv) and [$Ru_2(OAc)_4Cl$] (0.73g, 0.6 mmol). The round bottom flask was equipped with a short-path distillation head and the mixture was stirred and distilled until about 5 ml liquid left. Another 60 ml chlorobenzene was added to the flask and the mixture was distilled for a second time. This procedure was repeated for a total of twelve times. 50 ml 1:1 Et_2O/pentane solution was added to the remaining chlorobenzene mixture after the last distillation process. The solution was filtered through a sintered glass funnel. The filter cake was rinsed with 300 ml Et_2O until the filtrate ran

clear (pale yellow). The isolated solid was dried in a vacuum oven (80°C) and the resulting final product is burgundy red powder.

4.3.2. Temperature Controlled Ru-catalyzed C-H Amination and KIE Measurement

1 ml 1,2-dichloroethane, sulfamate (d_2-**4** for intramolecular KIE, β-d_1-**4** and d_2-**4** mixture for intermolecular KIE, 80 mg, 0.37 mmol), and bis(tert-butylcarbonyloxy)iodobenzene ($PhI(O_2{}^tCBu)_2$, 0.23g, 0.56 mmol, 1.5 equiv.) were mixed in a 5 ml Fisherbrand^{TM} class B glass vial with a stir bar. The reaction vial was incubated in a temperature regulated reaction chamber in the Mettler Toledo EasyMax 102 synthesis workstation. The reaction chamber was filled with aluminum bath beads for better heat conduction. After incubating for one hour, the reaction vial was added $Ru_2[hp]_4Cl$ (10mg, 0.016 mmol, 5 mol%). The reaction was initiated after the addition of the catalyst and allowed to proceed until substantial conversion had been reached. The time the experiment was performed and the percent conversion reached are given in **Table 8**.

Table 8. *The time for which the Ru-catalyzed C-H amination reacted for intramolecular and intermolecular KIE measurement of at various temperatures. (The percentage the reaction proceeded during the experimental period is included in the parenthesis.)*

	0 °C	20 °C	40 °C	60 °C	80 °C
KIE_{intra}	112 h (30%)	71 h (30%)	36 h (80%)	24 h (70%)	24 h (80%)
KIE_{inter}	--	--	--	--	12 h (67%)

After the temperature controlled reaction, the reaction mixture was cooled down and immediately filtered through a Büchner funnel that contains a 2cm-thick layer of Celite topped with a thin layer of basic alumina on the top of the filter paper. The filter cake was rinsed by 5ml ethyl ether. The filtrate was condensed under reduced pressure and the product(s) was purified by column chromatography (1.6:1 pentane: Et_2O). The product is not UV-active, so the TLC plate containing the product was visualized by heating after being treated with p-anisaldehyde stain (pink-light purple, Rf=0.38).

The isolated product was dissolved in 0.5 ml benzene and placed in an NORELL® 509-UP-7 5mm NMR tube. Overnight, the product would recrystallize out. The supernant that contained impurities (trace amount of the reactant that couldn't be separated from the column chromatography) was decanted. 0.5 ml 95:5 C_6H_6 : C_6D_6 was added to the NMR tube to dissolved the recrystallized product. The lowest amount deuterated solvent was used to increase the signal to noise ratio (S/N) in the ^2H NMR. The resulting sample was analyzed by taking ^1H-decoupled and ^2H-detected NMR spectra on the Bruker 600 MHz NMR. The longest T_1 measured for the deuterium signals is 0.2 sec (by the "inversion-recovery" method described in section 3.5.3). The parameters used to acquire the quantitative ^2H NMR spectra are: d_1=1.4 sec, p1= 150 μsec, plw1=6.6 W, plw12=0.027 W (for decoupling). The appropriate number of scans were used to make sure S/N > 500.

SUMMARY

This dissertation reported the research work that aims to rationalize the mechanism of synthetically useful and mechanistically interesting organic reactions by means of measuring and interpreting physical organic observables. The physical rule and molecular properties underlying the reactivity and selectivity of organic reactions uncovered by mechanistic study can be useful in guiding the design of enzyme inhibitor and new synthetic methodology.

Kinetic isotope effect is a very powerful physical organic observable for deciphering reaction mechanism, but require efficient experimental design and accurate interpretation. The research work on the Chugaev elimination, presented in chapter 2, unmasked the extraordinary secondary KIEs that are elevated by quantum tunneling, which suppressed the intramolecular KIEs which are previously considered to be "classical". The research project demonstrated our new method that extracts the primary and secondary KIEs from the intramolecular and intermolecular KIEs. The results indicate the need for a more robust model that can account for the multi-dimensionality of tunneling. The work on the Cope elimination, which is reported in chapter 3, indicate that kinetic complexity can result in "pseudo tunneling" phenomenon: temperature independence of the Arrhenius plot of the KIEs. Unfortunately, many enzyme-catalyzed and organometall-catalyzed reactions proceed through multiple steps and even exhibit several mechanistic pathways, cautions must be used when interpreting the temperature effect on KIE. The knowledge gained from studying the two prototype reactions (Chugaev elimination and Cope elimination) was applied to study the more exciting Ru-catalyzed C-H functionalization, presented in chapter 4. Experiments were designed and executed to probe the short-lived nitrenoid intermediate that dictates the chemoselectivity of the reaction. The study of magnetic effect upon the reaction generated negative results and showed the KIE may not be a sensitive observable for probing electronic multiplicity. Temperature dependence of the intramolecular KIE resembled the Chugaev elimination, implying the physical rules we learned for simple unimolecular elimination can be generalized to understand more complicated organic reactions.

REFERENCE

(1) Anslyn, E. V.; Dougherty, D. A. *Modern Physical Organic Chemistry*; University Science Books, 2006.

(2) Schramm, V. L. Transition States and Transition State Analogue Interactions with Enzymes. *Accounts of Chemical Research* **2015,** *48* (4), 1032.

(3) Ducati, R. G.; Namanja-Magliano, H. A.; Schramm, V. L. Transition-state inhibitors of purine salvage and other prospective enzyme targets in malaria. *Future medicinal chemistry* **2013,** *5* (11), 10.4155/fmc.13.51.

(4) Zhang, Y.; Evans, G. B.; Clinch, K.; Crump, D. R.; Harris, L. D.; Fröhlich, R. F. G.; Tyler, P. C.; Hazleton, K. Z.; Cassera, M. B.; Schramm, V. L. Transition State Analogues of Plasmodium falciparum and Human Orotate Phosphoribosyltransferases. *The Journal of Biological Chemistry* **2013,** *288* (48), 34746.

(5) Simmons, E. M.; Hartwig, J. F. On the Interpretation of Deuterium Kinetic Isotope Effects in C-H Bond Functionalizations by Transition-Metal Complexes. *Angewandte Chemie International Edition* **2012,** *51* (13), 3066.

(6) Milo, A.; Bess, E. N.; Sigman, M. S. Interrogating selectivity in catalysis using molecular vibrations. *Nature* **2014,** *507* (7491), 210.

(7) Glasstone, S.; Laidler, K. J.; Eyring, H. *The Theory of Rate Processes: The Kinetics of Chemical Reactions, Viscosity, Diffusion and Electrochemical Phenomena*; McGraw-Hill Book Company, Incorporated, 1941.

(8) Giagou, T.; Meyer, M. P. Mechanism of the Swern Oxidation: Significant Deviations from Transition State Theory. *The Journal of Organic Chemistry* **2010,** *75* (23), 8088.

(9) Oyola, Y.; Singleton, D. A. Dynamics and the Failure of Transition State Theory in Alkene Hydroboration. *Journal of the American Chemical Society* **2009,** *131* (9), 3130.

(10) Soudackov, A.; Hatcher, E.; Hammes-Schiffer, S. Quantum and dynamical effects of proton donor-acceptor vibrational motion in nonadiabatic proton-coupled electron transfer reactions. *The Journal of Chemical Physics* **2005,** *122* (1), 014505.

(11) Cukier, R. I. A Theory that Connects Proton-Coupled Electron-Transfer and Hydrogen-Atom Transfer Reactions. *The Journal of Physical Chemistry B* **2002,** *106* (7), 1746.

(12) Truhlar, D. G.; Isaacson, A. D.; Skodje, R. T.; Garrett, B. C. Incorporation of quantum effects in generalized-transition-state theory. *The Journal of Physical Chemistry* **1982,** *86* (12), 2252.

(13) Kohen, A.; Klinman, J. P. Enzyme Catalysis: Beyond Classical Paradigms. *Accounts of Chemical Research* **1998,** *31* (7), 397.

(14) Meyer, M. P. In *Advances in Physical Organic Chemistry*; Ian, H. W.;Nicholas, H. W., Eds.; Academic Press, 2012; Vol. Volume 46.

(15) Melander, L. C. S.; Saunders, W. H. *Reaction rates of isotopic molecules*; Wiley, 1980.

(16) Westheimer, F. H. The Magnitude of the Primary Kinetic Isotope Effect for Compounds of Hydrogen and Deuterium. *Chemical Reviews* **1961,** *61* (3), 265.

(17) Diem, M. In *Modern Vibrational Spectroscopy and Micro-Spectroscopy*; John Wiley & Sons, Ltd, 2015, DOI:10.1002/9781118824924.app5 10.1002/9781118824924.app5.

(18) Nguyen, Q.; Sun, K.; Driver, T. G. Rh2(II)-Catalyzed Intramolecular Aliphatic C–H Bond Amination Reactions Using Aryl Azides as the N-Atom Source. *Journal of the American Chemical Society* **2012,** *134* (17), 7262.
(19) Kwart, H. Temperature dependence of the primary kinetic hydrogen isotope effect as a mechanistic criterion. *Accounts of Chemical Research* **1982,** *15* (12), 401.
(20) Giagou, T.; Meyer, M. P. Kinetic Isotope Effects in Asymmetric Reactions. *Chemistry (Weinheim an der Bergstrasse, Germany)* **2010,** *16* (35), 10616.
(21) Kohen, A.; Klinman, J. P. Hydrogen tunneling in biology. *Chemistry & Biology* **1999,** *6* (7), R191.
(22) Bell, R. P. The Application of Quantum Mechanics to Chemical Kinetics. *Proceedings of the Royal Society of London. Series A* **1933,** *139* (838), 466.
(23) Bell, R. P. The tunnel effect correction for parabolic potential barriers. *Transactions of the Faraday Society* **1959,** *55* (0), 1.
(24) Zheng, J.; Zhang, S.; Lynch, B. J.; Corchado, J. C.; Chuang, Y.-Y.; Fast, P. L.; Hu, W.-P.; Liu, Y.-P.; Lynch, G. C.; Nguyen, K. A.et al.; 2010 ed. University of Minnesota, Minneapolis, NM, 2010.
(25) Bell, R. P. *The Tunnel Effect in Chemistry*; Springer US: New York, 1980.
(26) Stern, M. J.; Weston, R. E. Phenomenological manifestations of quantum‐mechanical tunneling. II. Effect on Arrhenius pre‐exponential factors for primary hydrogen kinetic isotope effects. *The Journal of Chemical Physics* **1974,** *60* (7), 2808.
(27) Stern, M. J.; Weston, R. E. Phenomenological manifestations of quantum‐mechanical tunneling. I. Curvature in Arrhenius plots. *The Journal of Chemical Physics* **1974,** *60* (7), 2803.
(28) Bigeleisen, J. Statistical Mechanics of Isotopic Systems with Small Quantum Corrections. I. General Considerations and the Rule of the Geometric Mean. *The Journal of Chemical Physics* **1955,** *23* (12), 2264.
(29) Decius, J. C.; Wilson, E. B. Sum Rules for the Vibration Frequencies of Isotopic Molecules. *The Journal of Chemical Physics* **1951,** *19* (11), 1409.
(30) Amin, M.; Price, R. C.; Saunders, W. H. Tunneling in elimination reactions. Tests of criteria for tunneling predicted by model calculations. *Journal of the American Chemical Society* **1990,** *112* (11), 4467.
(31) Saunders, W. H. Calculations of isotope effects in elimination reactions. New experimental criteria for tunneling in slow proton transfers. *Journal of the American Chemical Society* **1985,** *107* (1), 164.
(32) Wolfsberg, M.; Van Hook, W. A.; Paneth, P.; Rebelo, L. P. N. *Isotope Effects: in the Chemical, Geological, and Bio Sciences*; 1 ed.; Springer Netherlands, 2009.
(33) Xiang, S.; Meyer, M. P. A General Approach to Mechanism in Multiproduct Reactions: Product-Specific Intermolecular Kinetic Isotope Effects. *Journal of the American Chemical Society* **2014,** *136* (16), 5832.
(34) Bigeleisen, J. The Relative Reaction Velocities of Isotopic Molecules. *The Journal of Chemical Physics* **1949,** *17* (8), 675.
(35) Bigeleisen, J.; Mayer, M. G. Calculation of Equilibrium Constants for Isotopic Exchange Reactions. *The Journal of Chemical Physics* **1947,** *15* (5), 261.
(36) Frisch, M. J.; Trucks, G. W.; Schlegel, H. B.; Scuseria, G. E.; Robb, M. A.; Cheeseman, J. R.; Scalmani, G.; Barone, V.; Mennucci, B.; Petersson, G. A.et al.; Gaussian, Inc.: Wallingford, CT, USA, 2009.

(37) Zheng, J.; Zhang, S.; Corchado, J. C.; Chuang, Y.-Y.; Coitiño, E. L.; Ellingson, B. A.; Truhlar, D. G.; 2009-A ed. University of Minnesota, Minneapolis, Minnesota 55455, 2010.
(38) Baldridge, K. K.; Gordon, M. S.; Steckler, R.; Truhlar, D. G. Ab initio reaction paths and direct dynamics calculations. *The Journal of Physical Chemistry* **1989,** *93* (13), 5107.
(39) Zheng, J.; Truhlar, D. G.; POLYRATE, t. o., Ed. University of Minnesota, 2007.
(40) D G Truhlar, a.; Garrett, B. C. Variational Transition State Theory. *Annual Review of Physical Chemistry* **1984,** *35* (1), 159.
(41) Truhlar, D. G.; Isaacson, A. D.; Garrett, B. C. In *The Theory of Chemical Reaction Dynamics*; Baer, M., Ed.; CRC Press: Boca Raton, FL, 1985; Vol. 4.
(42) Truhlar, D. G.; Garrett, B. C. Variational transition-state theory. *Accounts of Chemical Research* **1980,** *13* (12), 440.
(43) Lu, D.-h.; Truong, T. N.; Melissas, V. S.; Lynch, G. C.; Liu, Y.-P.; Garrett, B. C.; Steckler, R.; Isaacson, A. D.; Rai, S. N.; Hancock, G. C.et al. POLYRATE 4: A new version of a computer program for the calculation of chemical reaction rates for polyatomics. *Computer Physics Communications* **1992,** *71* (3), 235.
(44) Truhlar, D. G. In *Isotope Effects In Chemistry and Biology*; Kohen, A.;Limbach, H.-H., Eds.; CRC Press, 2005.
(45) Skodje, R. T.; Truhlar, D. G.; Garrett, B. C. A general small-curvature approximation for transition-state-theory transmission coefficients. *The Journal of Physical Chemistry* **1981,** *85* (21), 3019.
(46) Skodje, R. T.; Truhlar, D. G.; Garrett, B. C. Vibrationally adiabatic models for reactive tunneling. *The Journal of Chemical Physics* **1982,** *77* (12), 5955.
(47) Bader, R. F. W.; Bourns, A. N. A KINETIC ISOTOPE EFFECT STUDY OF THE TSCHUGAEFF REACTION. *Canadian Journal of Chemistry* **1961,** *39* (2), 348.
(48) DePuy, C. H.; King, R. W. Pyrolytic Cis Eliminations. *Chemical Reviews* **1960,** *60* (5), 431.
(49) Nakagawa, M.; Kawahara, M. A Concise Synthesis of Physostigmine from Skatole and Activated Aziridine via Alkylative Cyclization. *Organic Letters* **2000,** *2* (7), 953.
(50) Hagiwara, H.; Kobayashi, K.; Miya, S.; Hoshi, T.; Suzuki, T.; Ando, M. The First Total Synthesis of (−)-Solanapyrone E Based on Domino Michael Strategy. *Organic Letters* **2001,** *3* (2), 251.
(51) Fu, X.; Cook, J. M. General approach for the synthesis of polyquinenes via the weiss reaction XII. The chugaev approach to ellacene (1,10-cyclododecanotriquinancene). *Tetrahedron Letters* **1990,** *31* (24), 3409.
(52) Kumamoto, T.; Tabe, N.; Yamaguchi, K.; Yagishita, H.; Iwasa, H.; Ishikawa, T. Synthetic studies on kinamycin antibiotics: elaboration of a highly oxygenated D ring. *Tetrahedron* **2001,** *57* (14), 2717.
(53) Meulemans, T. M.; Stork, G. A.; Macaev, F. Z.; Jansen, B. J. M.; de Groot, A. Total Synthesis of Dihydroclerodin from (R)-(−)-Carvone. *The Journal of Organic Chemistry* **1999,** *64* (25), 9178.
(54) Bach, R. D.; Andrzejewski, D.; Dusold, L. R. The Mechanism of the Cope elimination. *The Journal of Organic Chemistry* **1973,** *38* (9), 1742.
(55) Meyer, M. P.; DelMonte, A. J.; Singleton, D. A. Reinvestigation of the Isotope Effects for the Claisen and Aromatic Claisen Rearrangements: The Nature of the Claisen Transition States. *Journal of the American Chemical Society* **1999,** *121* (47), 10865.
(56) Kwart, H.; George, T. J.; Louw, R.; Ultee, W. Transition-state structures in sulfoxide and amine oxide thermolysis. *Journal of the American Chemical Society* **1978,** *100* (12), 3927.

(57) Kwart, L. D.; Horgan, A. G.; Kwart, H. Structure of the reaction barrier in the selenoxide-mediated formation of olefins. *Journal of the American Chemical Society* **1981,** *103* (5), 1232.
(58) Kwart, H.; Brechbiel, M. Role of solvent in the mechanism of amine oxide thermolysis elucidated by the temperature dependence of a kinetic isotope effect. *Journal of the American Chemical Society* **1981,** *103* (15), 4650.
(59) Saunders, W. H. Contribution of tunneling to secondary isotope effects in proton-transfer reactions. *Journal of the American Chemical Society* **1984,** *106* (7), 2223.
(60) Alhambra, C.; Gao, J.; Corchado, J. C.; Villà, J.; Truhlar, D. G. Quantum Mechanical Dynamical Effects in an Enzyme-Catalyzed Proton Transfer Reaction. *Journal of the American Chemical Society* **1999,** *121* (10), 2253.
(61) Hammett, L. P. The Effect of Structure upon the Reactions of Organic Compounds. Benzene Derivatives. *Journal of the American Chemical Society* **1937,** *59* (1), 96.
(62) Taft, R. W. Linear Steric Energy Relationships. *Journal of the American Chemical Society* **1953,** *75* (18), 4538.
(63) Harper, K. C.; Bess, E. N.; Sigman, M. S. Multidimensional steric parameters in the analysis of asymmetric catalytic reactions. *Nat Chem* **2012,** *4* (5), 366.
(64) Harper, K. C.; Vilardi, S. C.; Sigman, M. S. Prediction of Catalyst and Substrate Performance in the Enantioselective Propargylation of Aliphatic Ketones by a Multidimensional Model of Steric Effects. *Journal of the American Chemical Society* **2013,** *135* (7), 2482.
(65) Prasad, A. S. B.; Kanth, J. V. B.; Periasamy, M. Convenient methods for the reduction of amides, nitriles, carboxylic esters, acids and hydroboration of alkenes using NaBH4/I2system. *Tetrahedron* **1992,** *48* (22), 4623.
(66) Park, H. S.; Lee, H. Y.; Kim, Y. H. Facile Barton−McCombie Deoxygenation of Alcohols with Tetrabutylammonium Peroxydisulfate and Formate Ion. *Organic Letters* **2005,** *7* (15), 3187.
(67) Cope, A. C.; Foster, T. T.; Towle, P. H. Thermal Decomposition of Amine Oxides to Olefins and Dialkylhydroxylamines. *Journal of the American Chemical Society* **1949,** *71* (12), 3929.
(68) Kürti, L.; Czakó, B. *Strategic Applications of Named Reactions in Organic Synthesis: Background and Detailed Mechanisms*; Elsevier Academic Press, 2005.
(69) Cram, D. J.; McCarty, J. E. Studies in Sterochemistry. XXIV. The Preparation and Determination of Configuration of the Isomers of 2-Amino-3-phenylbutane, and the Steric Course of the Amine Oxide Pyrolysis Reaction in this System. *Journal of the American Chemical Society* **1954,** *76* (22), 5740.
(70) Remen, L.; Vasella, A. Conformationally Biased Mimics of Mannopyranosylamines: Inhibitors of ß-Mannosidases? *Helvetica Chimica Acta* **2002,** *85* (4), 1118.
(71) Kim, Y.; Kreevoy, M. M. The experimental manifestations of corner-cutting tunneling. *Journal of the American Chemical Society* **1992,** *114* (18), 7116.
(72) Davies, H. M. L.; Manning, J. R. Catalytic C-H functionalization by metal carbenoid and nitrenoid insertion. *Nature* **2008,** *451* (7177), 417.
(73) Davies, H. M. L.; Du Bois, J.; Yu, J.-Q. C-H Functionalization in organic synthesis. *Chemical Society Reviews* **2011,** *40* (4), 1855.
(74) Bergman, R. G. Organometallic chemistry: C-H activation. *Nature* **2007,** *446* (7134), 391.

(75) Labinger, J. A.; Bercaw, J. E. Understanding and exploiting C-H bond activation. *Nature* **2002,** *417* (6888), 507.
(76) Davies, H. M. L.; Beckwith, R. E. J. Catalytic Enantioselective C−H Activation by Means of Metal−Carbenoid-Induced C−H Insertion. *Chemical Reviews* **2003,** *103* (8), 2861.
(77) Davies, H. M. L. Recent Advances in Catalytic Enantioselective Intermolecular C-H Functionalization. *Angewandte Chemie International Edition* **2006,** *45* (39), 6422.
(78) Du Bois, J. Rhodium-Catalyzed C–H Amination. An Enabling Method for Chemical Synthesis. *Organic Process Research & Development* **2011,** *15* (4), 758.
(79) Wehn, P. M.; Du Bois, J. Enantioselective Synthesis of the Bromopyrrole Alkaloids Manzacidin A and C by Stereospecific C−H Bond Oxidation. *Journal of the American Chemical Society* **2002,** *124* (44), 12950.
(80) Fleming, J. J.; Du Bois, J. A Synthesis of (+)-Saxitoxin. *Journal of the American Chemical Society* **2006,** *128* (12), 3926.
(81) Hinman, A.; Du Bois, J. A Stereoselective Synthesis of (−)-Tetrodotoxin. *Journal of the American Chemical Society* **2003,** *125* (38), 11510.
(82) Davies, H. M. L.; Long, M. S. Recent Advances in Catalytic Intramolecular C-H Aminations. *Angewandte Chemie International Edition* **2005,** *44* (23), 3518.
(83) Dick, A. R.; Sanford, M. S. Transition metal catalyzed oxidative functionalization of carbon–hydrogen bonds. *Tetrahedron* **2006,** *62* (11), 2439.
(84) Harvey, M. E.; Musaev, D. G.; Du Bois, J. A Diruthenium Catalyst for Selective, Intramolecular Allylic C–H Amination: Reaction Development and Mechanistic Insight Gained through Experiment and Theory. *Journal of the American Chemical Society* **2011,** *133* (43), 17207.
(85) Stokes, B. J.; Richert, K. J.; Driver, T. G. Examination of the Mechanism of Rh2(II)-Catalyzed Carbazole Formation Using Intramolecular Competition Experiments. *The Journal of Organic Chemistry* **2009,** *74* (17), 6442.
(86) In *Fieser and Fieser's Reagents for Organic Synthesis*; Ho, T.-L.;Fieser, M.;Fieser, L., Eds.; Hoboken: John Wiley & Sons, Inc.
(87) Geisler, J.; Schneider, F.; Holguin, F. L.; Lovis, K.; Google Patents, 2006.

NMR SPECTRA

Agilent Technologies

Methyl_Xanthate

Sample Name	Methyl_Xanthate	Pulse sequence	s2pul	Temperature	30	Study owner	vnmr1
Date collected	2012-12-12	Solvent	cdcl3	Spectrometer	-vnmrs400	Operator	vnmr1

^{1}H NMR ($CDCl_3$, 400 MHz)

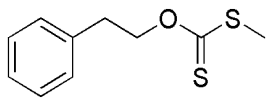

1

Agilent Technologies

D1-Methyl_Xanthate

Sample Name	D1-Methyl_Xanthate	Pulse sequence	s2pul	Temperature	30	Study owner	vnmr1
Date collected	2013-02-02	Solvent	cdcl3	Spectrometer	-vnmrs400	Operator	vnmr1

^{1}H NMR ($CDCl_3$, 400 MHz)

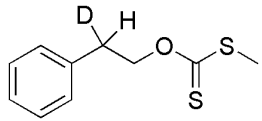

D_1-**1**

Agilent Technologies

xl_Exp209_DD_xanthate_AC

Sample Name	xl_Exp209_DD_xanthate_AC	Pulse sequence	PROTON	Temperature	23	Study owner	xiaoli
Date collected	2016-06-14	Solvent	cdcl3	Spectrometer	-vnmrs400	Operator	vnmr1

^{1}H NMR ($CDCl_3$, 400 MHz)

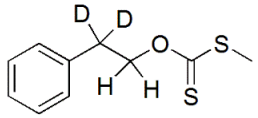

D_2-**1**

Agilent Technologies

CF3-amine-oxide_D2O

Sample Name	CF3-amine-oxide_D2O	Pulse sequence	PROTON	Temperature	20	Study owner	xiao
Date collected	2014-06-17	Solvent	d2o	Spectrometer	-vnmrs400	Operator	vnmr1

^{1}H NMR (D_2O, 400 MHz)

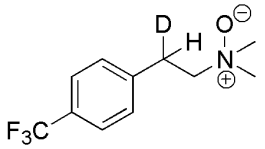

dl-**3-c**

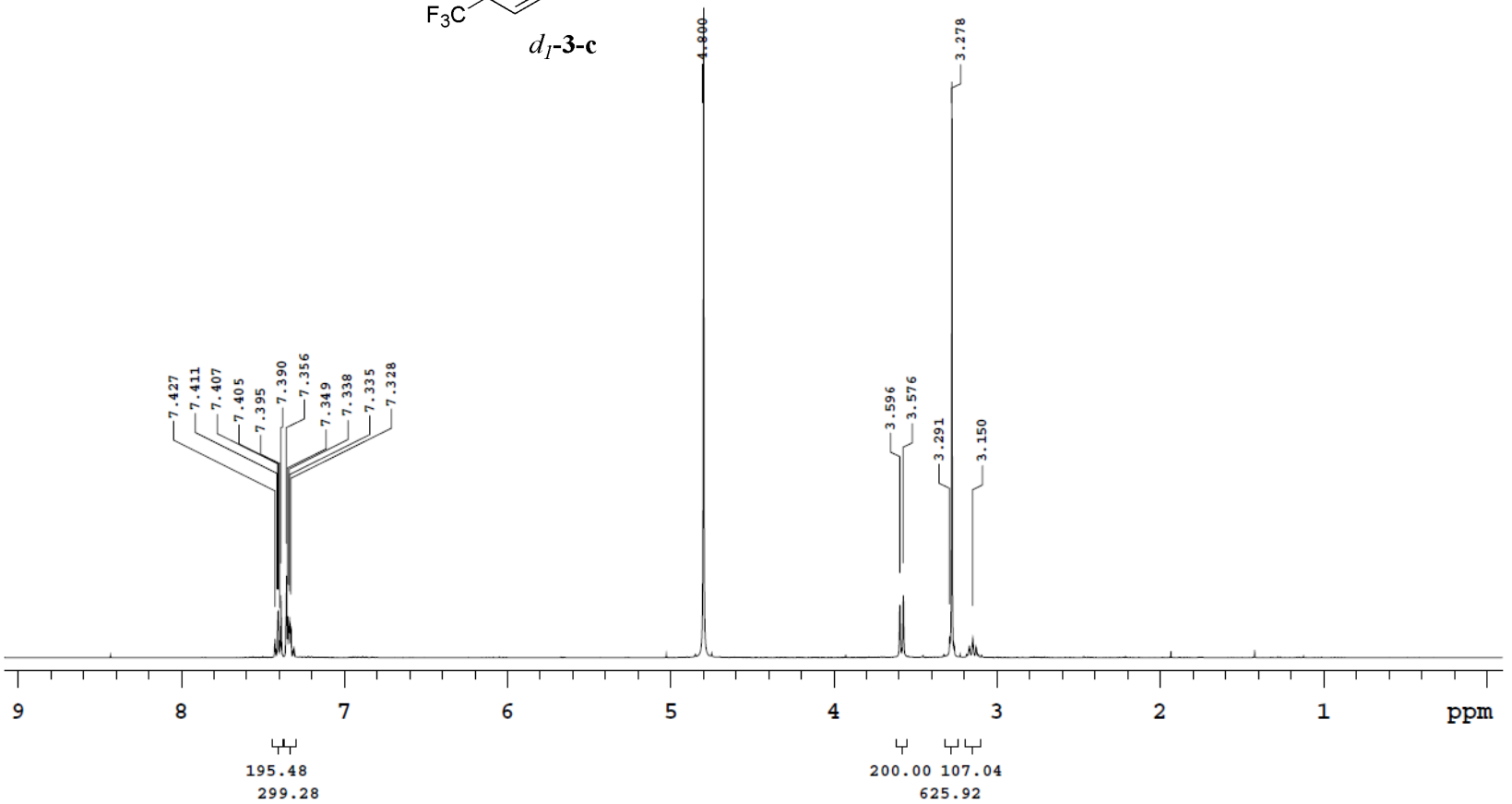

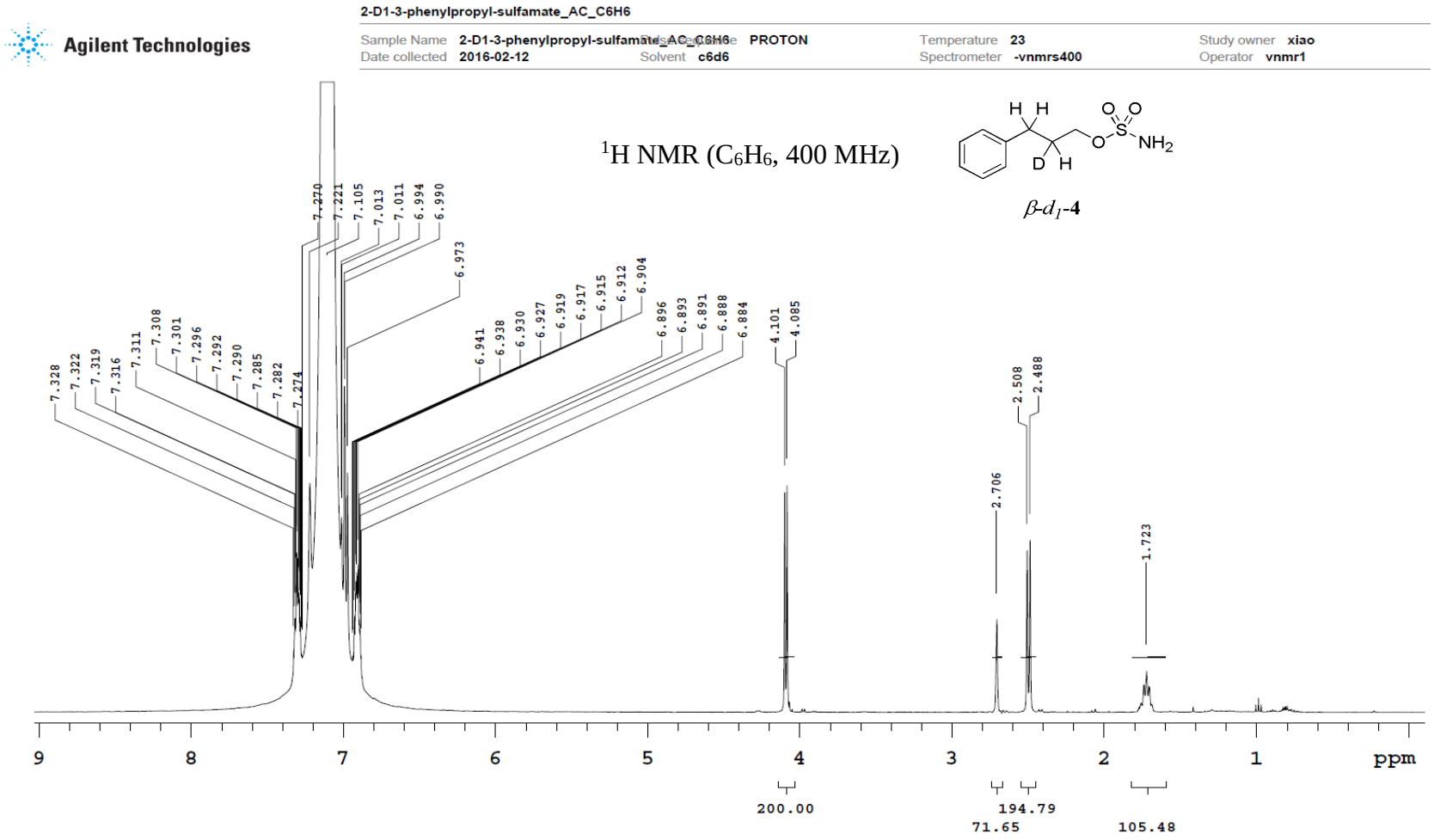
Agilent Technologies
2-D1-3-phenylpropyl-sulfamate_AC_C6H6
Sample Name 2-D1-3-phenylpropyl-sulfamate_AC_C6H6
Date collected 2016-02-12
Solvent c6d6
Temperature 23
Spectrometer -vnmrs400
Study owner xiao
Operator vnmr1
1H NMR (C6H6, 400 MHz)
β-d1-4
7.328
7.322
7.319
7.316
7.311
7.308
7.301
7.296
7.292
7.290
7.285
7.282
7.274
7.270
7.221
7.105
7.013
7.011
6.994
6.990
6.973
6.941
6.938
6.930
6.927
6.919
6.917
6.915
6.912
6.904
6.896
6.893
6.891
6.888
6.884
4.101
4.085
2.706
2.508
2.488
1.723
9
8
7
6
5
4
3
2
1
ppm
200.00
71.65
194.79
105.48

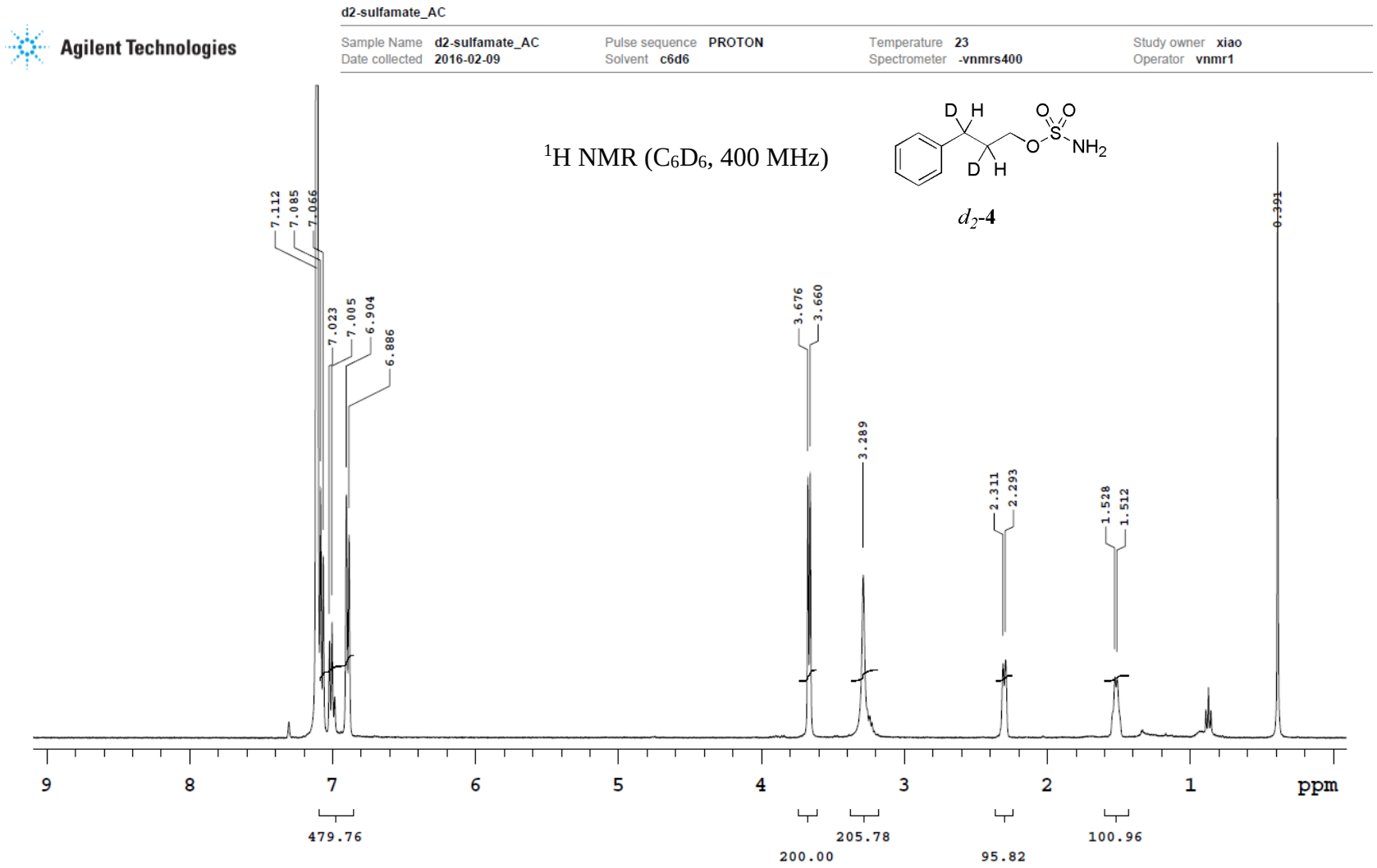
Agilent Technologies
d2-sulfamate_AC
Sample Name d2-sulfamate_AC
Date collected 2016-02-09
Pulse sequence PROTON
Solvent c6d6
Temperature 23
Spectrometer -vnmrs400
Study owner xiao
Operator vnmr1
^{1}H NMR (C_6D_6, 400 MHz)
d_2-4
7.112
7.085
7.066
7.023
7.005
6.904
6.886
3.676
3.660
3.289
2.311
2.293
1.528
1.512
0.391
9
8
7
6
5
4
3
2
1
ppm
479.76
200.00
205.78
95.82
100.96